An Adaptive Direct Conversion Transmitter

by
Derek S. Hilborn
B.A.Sc., Simon Fraser University, 1991

THESIS SUBMITTED IN PARTIAL FULFILLMENT OF
THE REQUIREMENTS FOR THE DEGREE OF
MASTER OF APPLIED SCIENCE
in the School of Engineering Science

SIMON FRASER UNIVERSITY

August 9, 1992

APPROVAL

NAME: Derek Hilborn

DEGREE: Master of Applied Science (Engineering Science)

TITLE OF THESIS: An Adaptive Direct Conversion Transmitter

EXAMINING COMMITTEE:

Chairman:

Dr. John Jones, P.Eng.
Associate Professor
School of Engineering Science, SFU

Senior Supervisor:

Dr. Shawn Stapleton, P.Eng.
Associate Professor
School of Engineering Science, SFU

Supervisor:

Dr. James Cavers, P.Eng.
Director
School of Engineering Science, SFU

Committee Member:

Dr. Paul Ho, P.Eng.
Associate Professor
School of Engineering Science, SFU

DATE APPROVED: 20.August 1992

PARTIAL COPYRIGHT LICENSE

I hereby grant to Simon Fraser University the right to lend my thesis, project or extended essay (the title of which is shown below) to users of the Simon Fraser University Library, and to make partial or single copies only for such users or in response to a request from the library of any other university, or other educational institution, on its own behalf or for one of its users. I further agree that permission for multiple copying of this work for scholarly purposes may be granted by me or the Dean of Graduate Studies. It is understood that copying or publication of this work for financial gain shall not be allowed without my written permission.

Title of Thesis/Project/Extended Essay

"An Adaptive Direct Conversion Transmitter"

Author: _____
(signature)

Derek S. Hilborn
(name)

August 20, 1992
(date)

ABSTRACT

An adaptive direct conversion transmitter is presented in which adjacent channel power measurements are used to simultaneously compensate for both power amplifier and quadrature modulator errors.

Three main contributions are given. First, analysis is presented which shows that adjacent channel power is a quadratic function of power amplifier nonlinearity as well as quadrature modulator errors. Quadrature modulator errors are gain imbalance, phase error, and DC offset errors. Second, a new optimization method is given which uses the predicted adjacent channel power surface to get fast convergence. Third, simulation and measured results are given for an adaptive system using offset QPSK modulation. The measured results confirm the analysis, and show that a 20 dB reduction in adjacent channel power is achievable.

In general, the adaptive direct conversion transmitter has applications in any system where power efficiency and spectral efficiency are important, and allows the use of smaller, more efficient power amplifiers in a direct conversion architecture.

ACKNOWLEDGEMENTS

First, I would like to thank my supervisors, Drs. Shawn Stapleton and James Cavers, for all their help and insight.

Secondly, my wife Jamie deserves a lot of credit for putting up with an academic, and understanding the demands of graduate research. Jamie gave me the reassurance and drive to keep going throughout this thesis. Quite literally, I could not have done it without her. Also thanks to our daughter, Alanda, who is five months old at the time of printing. Thanks for letting us get some sleep, baby!

Sirooj Rambaran deserves mention for his help in getting the hardware working, and for designing and building some of the essential parts. Thank you, Sirooj.

Finally, the students of the communications lab were great for bouncing ideas off of, and in creating an enjoyable working environment. In particular, Flaviu Costescu, Cameron Alakija and Le Quach deserve mention.

TABLE OF CONTENTS

APPROVAL ii

ABSTRACT iii

ACKNOWLEDGEMENTS iv

1 INTRODUCTION 1

2 BACKGROUND 5
2.1 Real Bandpass and Complex Envelope Notation 5
2.2 Quadrature Modulators 6
2.2.1 Quadrature Modulator Model 6
2.2.2 Quadrature Modulator Correction 8
2.3 Direct Conversion Architectures 9
2.3.1 RF Power Detector 9
2.3.2 Phase Detector 10
2.3.3 Cartesian Feedback 10
2.3.4 Adjacent Channel Power Detector 11
2.4 Linearization Techniques 11
2.4.1 Cartesian Feedback 11
2.4.2 Feed-forward 11
2.4.3 Linear Amplification Using Nonlinear Components 12
2.4.4 Predistortion 12
2.5 Optimization Methods 14

3 ANALYSIS 17
3.1 Analysis Model 17
3.2 Single Offset-Tone 19
3.3 Gaussian Input 22
3.3.1 Notation and Correlation Functions 22
3.3.2 Quadrature Modulator Autocorrelation 24
3.3.3 Power Amplifier Autocorrelation 26
3.3.4 Power Amplifier Spectrum 29
3.4 Summary of Analysis Results 31

4 ADAPTATION ALGORITHM 32
4.1 General Description 32
4.2 Adaptation by Recursive Least-Squared-Error Fit 33
4.3 Efficient Algorithm Calculations 35

5 SIMULATION 38
5.1 Simulation Model 38
5.1.1 Transmit Modem 38
5.1.2 Predistorter 39
5.1.3 Quadrature Modulator and Compensator 39
5.1.4 Power Amplifier 40
5.1.5 Power Detector 40
5.2 Adjacent Channel Power Dependence on Coefficients 41
5.3 Adaptation of Coefficients - Recursive Least Squares Algorithm 45

6 IMPLEMENTATION 48
6.1 System Overview 48
6.2 DSP Circuit 49
6.2.1 Transmit Modem 49
6.2.2 Predistorter 50
6.2.3 Quad Mod Compensator 50
6.3 Lowpass Filters 50
6.4 Quadrature Modulator 51
6.5 Quadrature Demodulator 52
6.6 Adjacent Channel Power Detector 52
6.7 Control Circuit 55

7 MEASURED RESULTS 57
7.1 Adjacent Channel Power Surface Plots 57
7.2 Spectrum Improvement 60
7.3 Convergence Speed 61

8 CONCLUSIONS 63

9 REFERENCES 65

APPENDIX A: HARDWARE SCHEMATICS 68

APPENDIX B: GAUSSIAN EXPANSION RESULTS 74

TABLE OF FIGURES

Figure 1.1 Direct Conversion Transmitter 1
Figure 1.2 Predistortion 2
Figure 1.3 Quadrature Modulator Correction 3
Figure 1.4 Adaptive Direct Conversion Transmitter 3
Figure 2.1 Quadrature Modulator 6
Figure 2.2 Quadrature Modulator Errors 7
Figure 2.3 Quadrature Modulator Correction Circuit 9
Figure 2.4 Quintic Polynomial Predistorter Circuit 14
Figure 3.1 Analysis Model 18
Figure 3.2 Output Spectrum for Single Offset-Tone Input 22
Figure 5.1 Simulation Model 38
Figure 5.2 Complex Gain of Class AB Amplifier 40
Figure 5.3 Power Detector Filter Frequency Response 41
Figure 5.4 Simulated Adj. Channel Power vs PD Coefficients 43
Figure 5.5 Simulated Adj. Channel Power vs QM Coefficients 44
Figure 5.6 Spectrum Improvement with Predistortion and QMC 46
Figure 5.7 RLS Algorithm Speed 47
Figure 6.1 Hardware Overview 48
Figure 6.2 Lowpass Filter Response 51
Figure 6.3 Power Detector Block Diagram 53
Figure 6.4 BPF1 Frequency Response 54
Figure 6.5 BPF2 Frequency Response 55
Figure 6.6 Control Circuit Block Diagram 56
Figure 7.1 Measured Adj. Channel Power vs PD Coefficients 58
Figure 7.2 Measured Adj. Channel Power vs QMC Coefficients 59
Figure 7.3 Measured Spectrum Improvement 60
Figure 7.4 Measured Convergence Speed 62

LIST OF TABLES

Table 3.1 Notation For Gaussian Analysis 24
Table 7.1 System Parameters for Measured Results 61

1 INTRODUCTION

Recently in mobile communications there has been considerable effort to revolutionize transceiver architectures to accommodate linear modulation techniques. As well, engineers continue research into more power efficient designs. The general approaches focus on utilizing some type of linearizer along with direct conversion transmitters, with the net objective being an improved spectral-power efficiency product.

A direct conversion architecture provides several desirable features. These features include reduced power consumption (increased efficiency) and reduced hardware complexity and size. Figure 1.1 illustrates a basic direct conversion transmitter. As shown, a transmit modem (TM) feeds a quadrature modulator (QM) which in turn drives a power amplifier (PA).

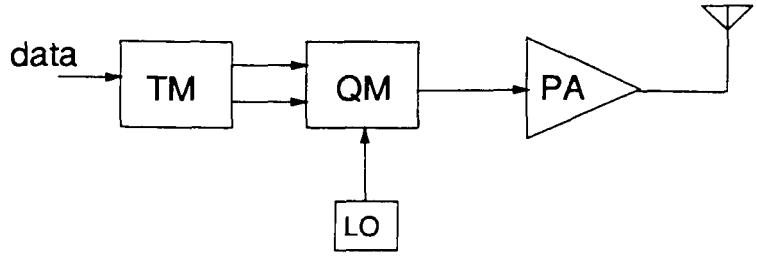

Figure 1.1 Direct Conversion Transmitter

Unfortunately, this simple transmitter is not practical for three main reasons. First, since power efficiency is one of the desired properties of the system, an efficient but nonlinear power amplifier must be used; to meet spectral efficiency demands the system requires some type of linearizer. Second, a direct conversion system is very sensitive to quadrature modulator gain imbalance, phase, and DC voltage offset errors; careful control over quadrature modulator errors is required. Third, both the power amplifier nonlinearity and the quadrature modulator errors can be expected to change with

temperature, channel frequency, device biasing and with component aging, and thus some means of monitoring the PA and QM performance is needed.

A successful direct conversion transmitter must therefore have (1) a linearizer, (2) control over quadrature modulator errors, and (3) adaptation of both (1) and (2) to maintain acceptable system performance. These requirements establish the design goals of the direct conversion transmitter.

Several linearization techniques have been studied such as Cartesian feedback, feedforward, LInear amplification using Nonlinear Components (LINC), and predistortion (PD). With predistortion, the signal to be amplified is passed through a nonlinear system whose characteristics are inverse to those of the power amplifier, as illustrated in Figure 1.2. If the two non-linearities are inverses of each other then the overall system will be linear.

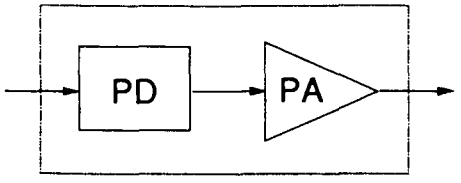

Figure 1.2 Predistortion

The second problem, quadrature modulator errors, is usually controlled using digital signal processing (DSP) techniques. A vector correction of the input signal compensates for errors in the quadrature modulator (Figure 1.3).

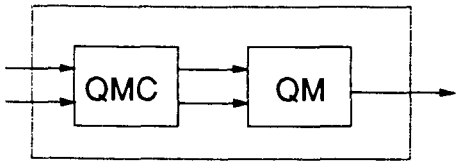

Figure 1.3 Quadrature Modulator Correction

Finally, since both the power amplifier and quadrature modulator characteristics change with temperature, biasing and frequency, both the predistorter and quadrature modulator correction must adapt to maintain acceptable performance quality. Analysis by Stapleton [1] Cavers [2] Kandola [3] and results from Costescu [4] showed that leakage of transmitted power into the adjacent channel is quadratically dependent on predistorter mis-adjustment and that measurement of this adjacent channel power can provide the necessary feedback in an adaptive predistorter system.

In this thesis, the use of adjacent channel power is expanded to include automatic correction for quadrature modulator errors. Figure 1.4 shows the new transmitter design.

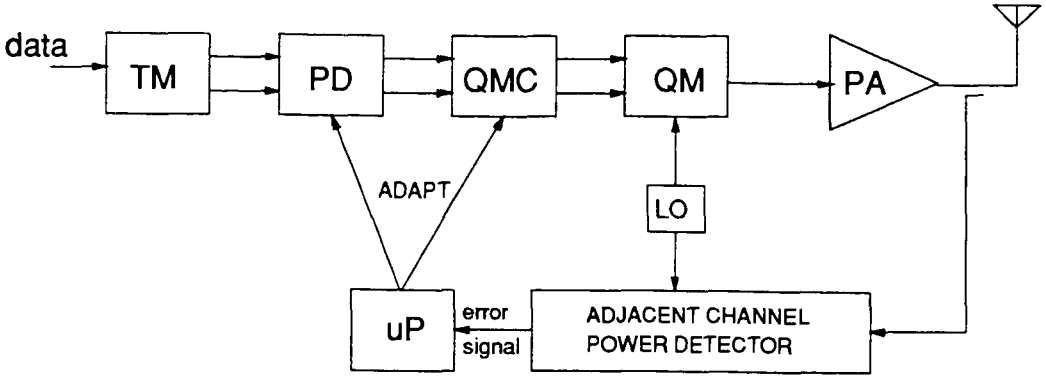

Figure 1.4 Adaptive Direct Conversion Transmitter

In the adaptive transmitter shown above, the transmit modem generates a complex baseband information signal which is predistorted and quadrature modulator compensated. The quadrature modulator then up-converts the signal to radio frequency (RF) where the power amplifier boosts the signal to drive an antenna. An adjacent channel power detector, coupled to the power amplifier output, delivers a DC error voltage to a micro-processor. The micro-processor then adjusts the predistorter and quadrature modulator compensator coefficients.

The main objective of this thesis work is (1) to establish the relationship between adjacent channel power and quadrature modulator coefficients, (2) to find a practical method with which to adjust the coefficients, (3) to implement the system in hardware. To this end, Section 2 provides relevant background material on quadrature modulators, direct conversion architectures, linearizers, and optimization methods. Section 3 outlines the analysis done to determine the relationship between quadrature modulator error and intermodulation power. A new surface-fit adaptation algorithm is discussed in Section 4, and Section 5 presents simulation results for a system like the one illustrated in Figure 1.4. Sections 6 and 7 give details of the hardware implementation and results for the adaptive system.

Several important results are obtained in this thesis. First, the adjacent channel power at the power amplifier output is analytically found to be a quadratic of both power amplifier non-linearity and quadrature modulator error. This result is verified both through simulation and with a real system. Second, a new adaptive algorithm utilizing the quadratic nature of intermodulation power is described. This new algorithm provides fast convergence and minimal processor memory and speed requirements. Finally, simulation and measured results are given to demonstrate the performance of the adaptive direct conversion system.

2 BACKGROUND

This section presents a review of current technology regarding direct conversion architectures, linearizers, and optimization methods. The concept of complex envelope and real bandpass notation is also introduced.

2.1 Real Bandpass and Complex Envelope Notation

Real bandpass signals are often used in the analysis and descriptive sections of this thesis. Complex envelope notation provides another way of dealing with real bandpass signals [5].

A real bandpass random process is expressed as

$$\tilde{Z}(t) = A(t) \cdot \cos[2\pi f_c t + \theta(t)]$$

where $A(t)$ and $\theta(t)$ are real-valued random processes. $\tilde{Z}(t)$ can also be written as

$$\begin{aligned}\tilde{Z}(t) &= Re\{A(t)\exp[j\theta(t)]\exp(j2\pi f_c t)\} \\ &= Re\{Z(t)\exp(j2\pi f_c t)\}\end{aligned}$$

where the *complex envelope* $Z(t)$ is given by

$$\begin{aligned}Z(t) &= A(t)\cos\theta(t) + jA(t)\sin\theta(t) \\ &= I(t) + jQ(t)\end{aligned}$$

Using the complex envelope components $I(t)$ and $Q(t)$ gives another representation of $\tilde{Z}(t)$:

$$\tilde{Z}(t) = I(t)\cos(2\pi f_c t) - Q(t)\sin(2\pi f_c t)$$

This last equation gives us the *real bandpass form* of $\tilde{Z}(t)$. This is precisely the form of a signal generated using quadrature modulation as discussed in the following section.

In general, a tilde over a signal name, $\tilde{Z}(t)$, will denote a real bandpass signal having a complex envelope of $Z(t)$.

2.2 Quadrature Modulators

Direct conversion systems are characterized by a single up-conversion stage using a high-frequency quadrature modulator. They have a high sensitivity to quadrature modulator gain imbalance, phase, and DC offsets errors. This section introduces the quadrature modulator model, its errors and compensation.

2.2.1 Quadrature Modulator Model

Figure 2.1 shows the quadrature modulator model.

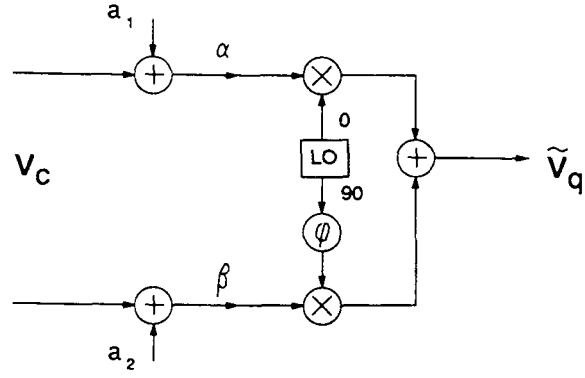

Figure 2.1 Quadrature Modulator

As shown, DC offsets a_1 and a_2 are added to the real and imaginary parts of the input signal. The real and imaginary parts of the signal then experience different gains of α and β, as well as a phase error of φ radians.

Quadrature modulator errors are troublesome since the errors distort the signal constellation and disturb the match between predistorter and power amplifier nonlinearities. The results of quad mod errors then is an increased bit-error-rate (BER) at the receiver and a spreading of the signal spectrum due to the nonlinearities of the power amplifier.

If quadrature modulator errors were more or less static, then a simple calibration of

the phase, gain and offset errors would suffice. However, quadrature modulator errors vary considerably with temperature, frequency, and with oscillator drive power. Figure 2.2 shows the sensitivity for Hewlett-Packard's HPMX-2001 850 MHz quadrature modulator [6]. Other quadrature modulators tested had comparable temperature and frequency sensitivities [7]. Appendix A shows the schematic for the Hewlett-Packard circuit.

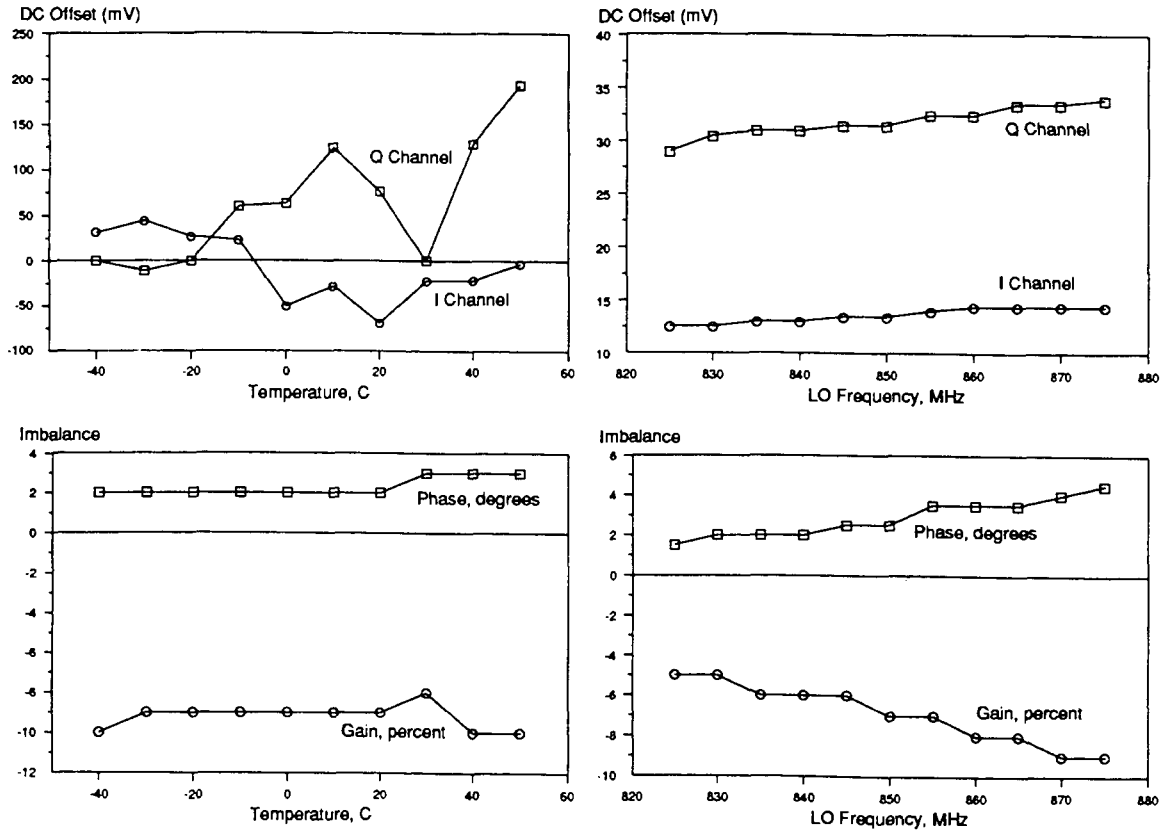

Figure 2.2 Quadrature Modulator Errors

The effect of quadrature modulator errors is modelled using matrix notation. Similar to the illustration of Figure 2.1, the quadrature modulator output $V_q(t)$ is given by

$$V_q(t) = M \cdot V_c(t) + M \cdot a \tag{2.2.1}$$

where

$$M = \begin{pmatrix} \alpha\cos(\phi/2) & \beta\sin(\phi/2) \\ \alpha\sin(\phi/2) & \beta\cos(\phi/2) \end{pmatrix}, \quad a = \begin{pmatrix} a_1 \\ a_2 \end{pmatrix} \tag{2.2.2}$$

and where the time variant signals are expressed as length two vectors composed of the signal's in-phase and quadrature parts. For example, *Z(t)* as described in Section 2.1 would be written as

$$Z(t) = \begin{pmatrix} I(t) \\ Q(t) \end{pmatrix}.$$

In the case of equation (2.2.2), the phase error has been split equally between the I and Q channels for symmetry. An equivalent representation in which the phase error is given completely to the quadrature channel is represented by the *M* matrix

$$M = \begin{pmatrix} \alpha & \beta\sin(\phi) \\ 0 & \beta\cos(\phi) \end{pmatrix}. \tag{2.2.3}$$

2.2.2 Quadrature Modulator Correction

Correction of quadrature modulator errors generally involves a vector correction of the input using DSP techniques. Quadrature modulator compensation (QMC) consists of a matrix multiplication of the complex baseband terms and the addition of suitable DC offsets. For a QMC input of $V_d(t)$, the corrected output is

$$V_c(t) = C \cdot V_d(t) + b \tag{2.2.4}$$

where

$$C = M^{-1} = \frac{\sec\phi}{\alpha\beta}\begin{pmatrix} \beta\cos(\phi/2) & -\beta\sin(\phi/2) \\ -\alpha\sin(\phi/2) & \alpha\cos(\phi/2) \end{pmatrix} \quad \text{and} \quad b = -a \tag{2.2.5}$$

correspond to *M* in equation (2.2.1). With equation (2.2.3) as a starting point, C becomes

$$C = M^{-1} = \frac{\sec\phi}{\alpha\beta}\begin{pmatrix} \beta\cos(\phi) & -\beta\sin(\phi) \\ 0 & \alpha \end{pmatrix}. \tag{2.2.6}$$

Figure 2.3 below represents the correction circuit comparable to equations (2.2.4) and (2.2.6).

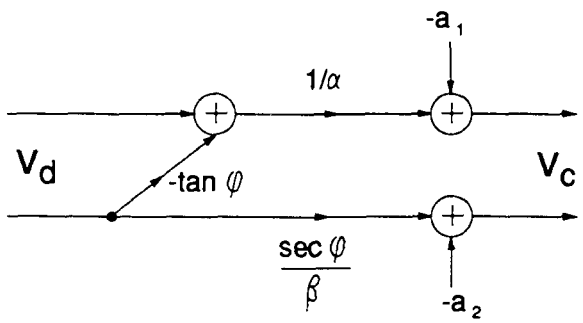

Figure 2.3 Quadrature Modulator Correction Circuit

The above correction is similar to the one used by Faulkner [8], as discussed in the next section, Direct Conversion Architectures.

2.3 Direct Conversion Architectures

Several architectures which deal with quadrature modulator problems in direct conversion systems are discussed in the literature [8, 9, 10]. These systems were the RF power detector method, the phase comparator method, and the Cartesian feedback method. The new architecture based on adjacent channel power measurements is also mentioned.

2.3.1 RF Power Detector

Faulkner [8] provides for automatic adjustment of quadrature modulators. In his method, a diode detector measures the RF power corresponding to a set of test vectors. From these measurements the quadrature modulator's errors are calculated, and the correction circuit is suitably adjusted. This method unfortunately requires periodic interrupts in the transmitted output so the test vectors are not transmitted.

The need for special test vectors can be eliminated by sampling the detector at the correct point in the trajectory of the incoming modulation, i.e. when the signal crosses the I or Q axis. This modification requires delay calibration in the detector, and is suited to modulation formats having quadrature symmetry.

2.3.2 Phase Detector

A novel technique by Telliez [9] implemented on a monolithic circuit uses a phase comparator to automatically adjust the quadrature phase. The phase comparator requires calibration, though, and may be sensitive to temperature and supply voltage changes.

The design provides the possibility of adjusting amplitudes, but no means of automatically doing so is offered by the author. Also, the problem of DC voltage offsets is not mentioned in the paper.

2.3.3 Cartesian Feedback

Cartesian feedback, described by Bateman [10] is normally used for linearization. However, it can also correct quadrature modulator errors. Bateman's system uses a down-converted output signal to apply negative feedback at the input of the system. The transmitter uses a quadrature demodulator to do the down-conversion.

This system has two limitations. First, stability may be a problem since loop phase delay must remain below 180° to prevent oscillations. The loop delay problem limits the loop gain and bandwidth which in turn limit linearity and stability. Secondly, the quadrature demodulator introduces gain, phase, and DC offset errors. One solution to the DC offset problem is a periodic nulling of the offsets with the transmitter turned off. Operationally this solution is not too attractive.

2.3.4 Adjacent Channel Power Detector

The new method presented in this thesis is based the measurement of adjacent channel power. As analysis, simulation, and measurements show (Chapters 3, 5, and 7), when a quadrature modulator is followed by a non-linear power amplifier, the amount of transmitted power which spills into the adjacent channel space is a quadratic function of the quadrature modulator error. In the new method, an adjacent channel power detector provides feedback to a microprocessor. The microprocessor adjust a correction circuit until a power minimum is measured by the detector, at which time the optimum setting has been found.

The adjacent channel power detector method is not sensitive to loop delay since the correction is not a real time operation; a slow adaptation speed is sufficient since the quadrature modulator (and power amplifier) change slowly in time.

2.4 Linearization Techniques

Four types of linearization techniques are common in the literature. These include Cartesian feedback, feedforward, LINC, and predistortion.

2.4.1 Cartesian Feedback

The Cartesian feedback loop described in Section 2.3.3 is also used to linearize a power amplifier. The same limitations mentioned earlier also apply to the linearization application – the stability problems and quadrature demodulator errors limit performance.

2.4.2 Feed-forward

Feed-forward linearization [11] uses a delayed version of the input signal and the power amplifier output (with the same delay) to generate an error signal. This error signal is further amplified and subtracted from the power amplifier output.

The feed-forward method has shown good linearization abilities, but tends to be expensive and sensitive since the transmitter hardware is doubled and the phase delay circuits must be accurately calibrated.

2.4.3 Linear Amplification Using Nonlinear Components

Linear Amplification Using Nonlinear Components [12], or LINC, uses the fact that an arbitrary bandpass signal can be decomposed into two constant envelope, angle modulated signals. Constant envelope signals can be amplified using nonlinear amplifiers because the amplifiers are run at a constant input power. With LINC, the input signal is split into the two constant envelope signals, each of which is amplified separately. Then the amplifier outputs are combined to form the desired output signal.

LINC transmitters are sensitive because the two amplifiers must be carefully matched in gain and phase. The efficiency of LINC linearizers is reduced by losses in the power combiner at the transmitter output, but class C amplifiers can be used.

2.4.4 Predistortion

Predistortion has been studied extensively in the literature [1-4,13,14]. As previously illustrated in Figure 1.2, a predistorter having inverse characteristics to those of the power amplifier 'pre-distorts' the input signal before amplification so the overall output is linear with respect to the input. Predistortion can be implemented at RF, IF, or at baseband, and either analog of digital technologies can be applied.

Cavers [14] models the amplifier as a memoryless nonlinearity with level dependent complex gain. That is, the complex envelope of its input V_i and output V_a are related by

$$V_a = V_i G(|V_i|^2) = V_i G(X_i) \tag{2.4.1}$$

where X_i denotes the magnitude squared of V_i, and $G(X_i)$, the complex gain of the amplifier.

The gain-based predistorter is used in this thesis, both in simulation and in the constructed system. The input-output relationship of the predistorter is given by

$$V_p = V_m F(|V_m|^2) = V_m F(X_m) \tag{2.4.2}$$

where the input is V_m and the predistorter output is V_p. $F(X_m)$ denotes the complex gain of the predistorter, and X_m, the magnitude squared of V_m.

Two approaches have been used to implement the gain based predistorter. In one [14], a look-up table having input power as the index and complex gain as the table entry is used. The table look-up method can be used to fit any gain profile, and performance can be adjusted by increasing or decreasing the table size. The second approach [3,4] uses two polynomial equations to fit the desired complex gain curves. This method is simpler to implement, but arbitrary gain profiles may be difficult to fit with polynomial functions. The polynomial method, because it has fewer variables, is also easier to initialize and update than the table look-up method.

Costescu [4] has achieved good results with a fifth order (quintic) polynomial predistorter. Figure 2.4 below illustrates the predistorter.

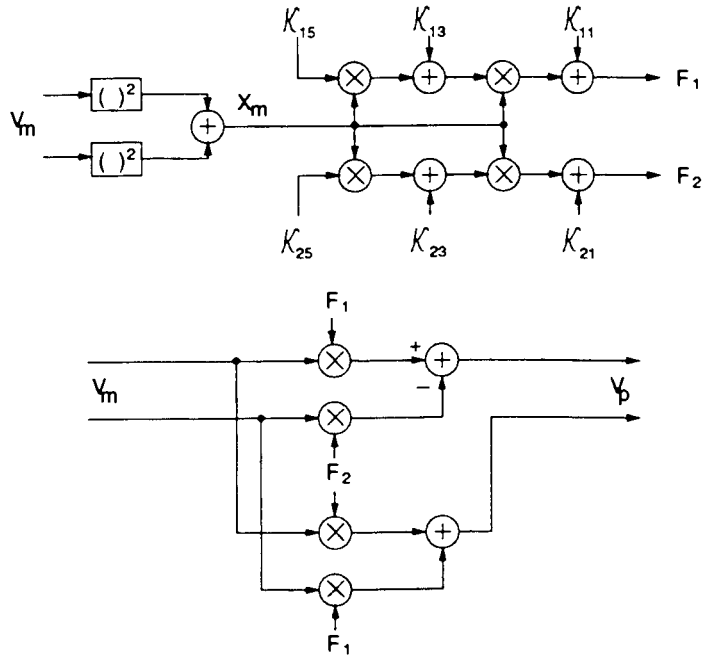

Figure 2.4 Quintic Polynomial Predistorter Circuit

The above system implements equations (2.4.2) where $F = F_1 + jF_2$ and

$$F_1(X_m) = \kappa_{11} + \kappa_{13} \cdot X_m + \kappa_{15} \cdot X_m^2 \tag{2.4.3}$$

$$F_2(X_m) = \kappa_{21} + \kappa_{23} \cdot X_m + \kappa_{25} \cdot X_m^2$$

giving an output

$$V_p = \kappa_1 V_m + \kappa_3 V_m^3 + \kappa_5 V_m^5. \tag{2.4.4}$$

where $\kappa_1 = \kappa_{11} + j\kappa_{21}$, $\kappa_3 = \kappa_{13} + j\kappa_{23}$, and $\kappa_5 = \kappa_{15} + j\kappa_{25}$.

2.5 Optimization Methods

Typical systems under normal operating conditions will experience some changes in their characteristics. In the case of the power amplifier, we expect the complex gain to change with device aging, with temperature changes, and with power supply variations.

With quadrature modulators, we expect the DC offsets, gain imbalance and phase error to change with temperature, aging, and LO power (Figure 2.2 illustrates two of these changes).

To maintain a good match between the predistorter and power amplifier (for example), the system must be able to adapt to the changing conditions. Many optimization methods can be used to do the adaptation, but the algorithms can be classified into three categories: direct search, gradient, and surface fit methods.

(1) Direct Search Methods: Direct search methods are simple, robust means of unconstrained optimization. In these methods, trial measurements (an exploration) around the present position find local differences in the function's value. If a trial measurement locates a better solution, then the new position is recorded and the algorithm proceeds. At some point the exploration will fail to find a better function value, and either the exploration area will be decreased, or the optimization will stop.

Although direct search methods are simple to implement, their convergence times are comparatively slow. An example of a direct search method is Hooke and Jeeves' method [15].

(2) Gradient Methods: Methods which use the slope of the function to optimize the variables are called gradient methods. Algorithms like the steepest descent technique move in the gradient direction giving the fastest decrease in the function value [16]. While gradient methods are faster than direct search methods, they suffer from sensitivity problems due to approximations in calculating the gradients. The gradient approximations are further distorted when the measurements contain random noise.

*(3) **Surface Fit Methods***: Surface fit techniques use information about the function to predict the position of the minimum from only a few measured points. For example, if one knows that a one-variable function is quadratic, then only three measurements are needed (in a noiseless environment) to find the function minimum. Surface fit methods, while achieving fast convergence, may also require a significant increase in complexity. In Section 4 a surface fit technique is described in detail.

3 ANALYSIS

The analysis in this section is used to determine the relationship between power amplifier nonlinearity, quadrature modulator errors, and the power amplifier output spectrum. The output spectrums are determined for two input signals: (1) single offset-tone, and (2) Gaussian stationary random signals. In the first case, the output spectrum is calculated, and then verified with simulation. In the second case, autocorrelation functions and Fourier transforms are used to determine the output spectrum.

3.1 Analysis Model

To keep the analysis manageable, a simple model composed of a quadrature modulator and power amplifier is used, as illustrated in Figure 3.1. The power amplifier output is modeled using the third order equation

$$\begin{aligned} V_a(t) &= \zeta_1 V_q(t) + \zeta_3 V_q(t)^3 \\ &= V_q(t) G(X_q(t)) \end{aligned} \tag{3.1.1}$$

where $X_q = V_q^2$, $G(X_q) = \zeta_1 + \zeta_3 X_q$, and ζ_1, ζ_3 are complex real numbers.

The quadrature modulator model is as in Section 2.2. DC offsets a_1 and a_2, I and Q channel gains of α and β, and phase error of φ describe the quadrature modulator. In the analysis, the gain ratio α/β in the quadrature modulator is defined as $(1+\varepsilon)$ so that the gain imbalance is simply ε. DC offset values are given as percentages of the desired signal's amplitude. The phase error is measured in radians. Furthermore, to maintain a constant signal power we set $\alpha^2 + \beta^2 = 2$.

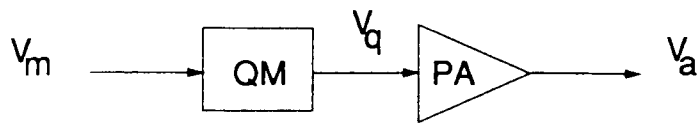

Figure 3.1 Analysis Model

The system of Figure 3.1 is noticeably simpler than the system proposed in the introduction (Figure 1.4, page 3). It can be shown, however, that this simpler system gives results which can be applied to the more complex one. For example, it's easy to show that the QMC and QM can be combined to form a *composite* quadrature modulator. If the QMC corrects for gain error ε', phase error φ', and DC offset errors a', and the QM has errors ε, φ, and a, then the composite system has errors of approximately ε", φ", and a" where

$$\varepsilon'' \approx \varepsilon - \varepsilon'$$

$$\phi'' \approx \phi - \phi'$$

$$a'' = a - a'.$$

Clearly, the composite system behaves like a single QM, but with adjustable gain, phase, and DC offset errors. Similarly, Kandola [3] showed that a predistorter-power amplifier system could be expressed as a single, adjustable nonlinear system.

Another simplification is the choice of input signals. Neither pure tone nor Gaussian inputs are very good representations of a single data signal. However, these signals are bounding cases of data signals, and thus the results for tone and Gaussian modulation will be suggestive of the results for real data signals.

3.2 Single Offset-Tone

Single offset-tone modulation is perhaps the simplest way to start the analysis. In this section, the output spectrum is calculated for an offset-tone fed through a quadrature modulator (with errors) and through a nonlinear power amplifier.

The input signal V_m is expressed as

$$V_m(t) = A\exp(jw_0t) = \begin{pmatrix} A\cos(w_0t) \\ A\sin(w_0t) \end{pmatrix}. \tag{3.2.1}$$

Using the symmetric matrix of equation (2.2.2) gives the quadrature modulator output $V_q(t)$:

$$V_q(t) = M \cdot V_m + M \cdot a. \tag{3.2.2}$$

Since the quadrature modulator is a linear device, the two components of V_q can be calculated separately and the results summed. Ignoring the DC offsets initially gives $V_{q1}(t)$:

$$\begin{aligned} V_{q1}(t) &= \begin{pmatrix} \alpha\cos(\phi/2) & \beta\sin(\phi/2) \\ \alpha\sin(\phi/2) & \beta\cos(\phi/2) \end{pmatrix} \bullet \begin{pmatrix} A\cos(w_0t) \\ A\sin(w_0t) \end{pmatrix} \\ &= A[\alpha\cos(\phi/2) + j\alpha\sin(\phi/2)]\cos(w_0t) \\ &\quad + A[\beta\sin(\phi/2) + j\beta\cos(\phi/2)]\sin(w_0t). \end{aligned} \tag{3.2.3}$$

The second part of $V_q(t)$, obtained by considering the DC offset terms, is $V_{q2}(t)$.

$$V_{q2}(t) = \begin{pmatrix} \alpha\cos(\phi/2) & \beta\sin(\phi/2) \\ \alpha\sin(\phi/2) & \beta\cos(\phi/2) \end{pmatrix} \bullet \begin{pmatrix} a_1 \\ a_2 \end{pmatrix} \tag{3.2.4}$$

Adding equation (3.2.3) and (3.2.4) and taking the Fourier transform [17] gives the frequency equation, $V_q(w)$

$$V_q(w) = \pi A\left[\alpha\cos\left(\frac{\phi}{2}\right) + j\alpha\sin\left(\frac{\phi}{2}\right)\right](\delta(w+w_0) + \delta(w-w_0))$$
$$+ j\pi A\left[\beta\sin\left(\frac{\phi}{2}\right) + j\beta\cos\left(\frac{\phi}{2}\right)\right](\delta(w+w_0) - \delta(w-w_0)) \qquad (3.2.5)$$
$$+ 2\pi A\left[\alpha\cos\left(\frac{\phi}{2}\right)a_1 + \beta\sin\left(\frac{\phi}{2}\right)a_2 + j\alpha\sin\left(\frac{\phi}{2}\right)a_1 + j\beta\cos\left(\frac{\phi}{2}\right)a_2\right]\delta(w)$$

where δ is the dirac-delta function [17]. Simplifying (3.2.5) by keeping only the lowest order terms (order < 3) gives the following magnitude-spectrum equation:

$$\frac{|V_q(w)|}{2\pi A} \approx \left(\frac{\varepsilon^2+\phi^2}{4}\right)^{1/2}\delta(w+w_0) + (a_1^2+a_2^2)^{1/2}\delta(w) + \delta(w-w_0). \qquad (3.2.6)$$

The power amplifier output is calculated next. Using the third order model, the amplifier output is given by

$$V_a(t) = V_q(t)\left[\zeta_1 + \zeta_3 \cdot (X_q(t))\right] \qquad (3.2.7)$$

where $X_q(t) = |V_q(t)|^2$.

Convolution provides a convenient graphical way to find the output spectrum. The spectrum corresponding to $|V_q|^2$ is $V_q(w) \otimes V_q(-w)^*$ where the ($\otimes$) represents convolution and the (*) represents the complex conjugate. Using the approximation of equation (3.2.6), convolution of the δ functions occur, yielding (3.2.8):

$$\frac{|V_q(w) \otimes V_q(-w)^*|}{2\pi A^2} \approx \left(\frac{\varepsilon^2+\phi^2}{4}\right)^{1/2}(\delta(w+2w_0) + \delta(w-2w_0))$$
$$+ (a_1^2+a_2^2)^{1/2}(\delta(w+w_0) + \delta(w-w_0)) \qquad (3.2.8)$$
$$+ \delta(w-w_0)).$$

Convolving V_q with its square gives the third order result:

$$\frac{|V_q(w)\otimes V_q(-w)^*\otimes V_q(w)|}{2\pi A^3} \approx (y^2)\delta(w+3w_0)+(2xy)\delta(w+2w_0)$$
$$+(2y)\delta(w+w_0)+(2x)\delta(w) \qquad (3.2.9)$$
$$+\delta(w-w_0)+(x)\delta(w-2w_0)$$
$$+(y)\delta(w-3w_0)$$

where
$$x=(a_1^2+a_2^2)^{1/2}, \quad y=\left(\frac{\varepsilon^2+\phi^2}{4}\right)^{1/2}. \qquad (3.2.10)$$

To obtain the final result, the linear term (3.2.6) and the cubic term (3.2.9) are scaled by factors ζ_1 and ζ_3, respectively, and summed. Keeping only the most significant terms yields the following result, the power amplifier output spectrum:

$$\frac{|V_a(w)|}{2\pi A} \approx |\zeta_3|\,(A^2y^2)\delta(w+3w_0)+|\zeta_3|\,(2A^2xy)\delta(w+2w_0)$$
$$+|\zeta_1|\,(y)\delta(w+w_0)+|\zeta_1|\,(x)\delta(w) \qquad (3.2.11)$$
$$+|\zeta_1|\,\delta(w-w_0)+|\zeta_3|\,(A^2x)\delta(w-2w_0)$$
$$+|\zeta_3|\,(A^2y)\delta(w-3w_0).$$

The variables x and y are as defined in equation (3.2.10). Equation (3.2.11) shows that for tone modulation the out-of-channel power at $\pm 2w_0$ and $\pm 3w_0$ is quadratically dependent on both quadrature modulator error and on power amplifier nonlinearity, although the dependence is separate.

Equation (3.2.11) was verified numerically with ζ_1 set to 1.0, ζ_3 set to 0.1 - 0.1j, and with 5% offsets, 0.05 radian phase error, and 5% gain error. The approximated spectrum for this combination is shown in Figure 3.2 below. The approximated power levels are within 2dB of the calculated values. The differences in calculated and approximated results are due to two errors: one, the approximations themselves, and two, errors associated with neglecting the relative phases of the signals.

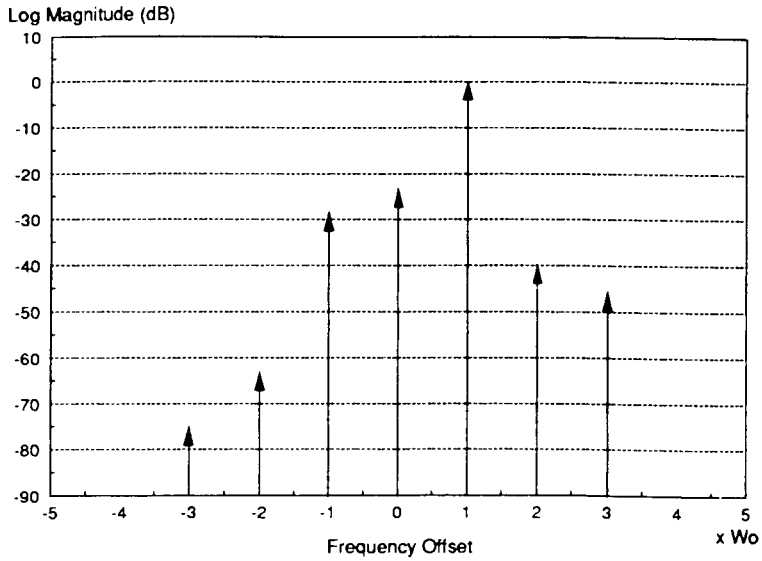

Figure 3.2 Output Spectrum for Single Offset-Tone Input

3.3 Gaussian Input

For single offset-tone modulation the adjacent channel power was quadratically dependent on quadrature modulator error and on power amplifier nonlinearity. This section shows that a stationary Gaussian input signal with zero-mean also produces adjacent channel power with a quadratic dependence on errors. The basic approach is to calculate the autocorrelation function at the quadrature modulator and power amplifier outputs, and then calculate the output spectrum from the amplifier autocorrelation function.

The model used in the analysis is the same as for Section 3.1, and is illustrated in Figure 3.1.

3.3.1 Notation and Correlation Functions

The input complex envelope $V_m(t)$ is assumed to be a wide-sense stationary (WSS) Gaussian random variable with zero-mean, as defined in [5]. $V_m(t)$ is written as

$$V_m(t) = i(t) + jq(t). \tag{3.3.1}$$

Since $V_m(t)$ is zero-mean, so are both $i(t)$ and $q(t)$. The auto- and cross-correlation functions of $i(t)$ and $q(t)$ are defined as

$$\begin{aligned} R_{ii}(\tau) &\equiv E\{i(t)i(t+\tau)\} \\ R_{qq}(\tau) &\equiv E\{q(t)q(t+\tau)\} \\ R_{iq}(\tau) &\equiv E\{i(t)q(t+\tau)\} \\ R_{qi}(\tau) &\equiv E\{q(t)i(t+\tau)\}. \end{aligned} \tag{3.3.2}$$

The stationarity of $V_m(t)$ implies that the correlation functions satisfy the following properties [18]:

$$\begin{aligned} R_{ii}(\tau) &= R_{qq}(\tau) \\ R_{iq}(\tau) &= -R_{qi}(\tau) = R_{qi}(-\tau) = -R_{iq}(-\tau). \end{aligned} \tag{3.3.3}$$

The autocorrelation $R_m(\tau)$ is by definition

$$R_m(\tau) \equiv \frac{1}{2} E\{V_m(t)V_m^*(t+\tau)\} \tag{3.3.4}$$

which can be shown, using linearity and the properties of (3.3.3), to be equivalent to

$$R_m(\tau) = R_{ii}(\tau) - jR_{iq}(\tau). \tag{3.3.5}$$

The quadrature modulator and amplifier outputs are determined in terms of $R_m(\tau)$ in the next sections. In order to simplify the following discussions and equations, the notation used is summarized in the following table.

TABLE 3.1 Notation for Gaussian Analysis

DESCRIPTION	NOTATION	at time t	at time t+τ
Re($V_m(t)$)	$i(t)$	i_1	i_2
Im($V_m(t)$)	$q(t)$	q_1	q_2
Re($V_q(t)$)	$x(t)$	x_1	x_2
Im($V_q(t)$)	$y(t)$	y_1	y_2
DC offsets at QM output	$\mu = \mu_1 + j\mu_2$		
Autocorrelation of $V_m(t)$	$R_m(\tau)$		
Autocorrelation of Re($V_m(t)$)	$R_{ii}(\tau)$		
Autocorrelation of Im($V_m(t)$)	$R_{qq}(\tau)$		
Cross Correlation of Re($V_m(t)$),Im($V_m(t)$)	$R_{iq}(\tau)$		
Autocorrelation of zero-mean part of $V_q(t)$	$Rq(\tau)$		
Autocorrelation of $V_a(t)$	$R_a(\tau)$		

3.3.2 Quadrature Modulator Autocorrelation

The quadrature modulator's output, $V_q(t)$, is a linear combination of the real and imaginary parts of the input, $V_m(t)$, so finding the correlation functions is straight forward. However, the output is not zero-mean since the quadrature modulator adds DC offsets. To make the quadrature modulator output zero-mean again, we simply consider the quadrature modulator output as the sum of two signals – one a zero-mean Gaussian stationary random signal, and the other a constant.

The autocorrelation function of the zero-mean, real part of the quadrature modulator output is found as follows:

$$Rq_{ii}(\tau) \equiv E\{Re(V_q(t))Re(V_q(t+\tau))\}$$
$$= E\left\{\left(\alpha\cos\left(\frac{\phi}{2}\right)i_1 + \beta\sin\left(\frac{\phi}{2}\right)q_1\right)\left(\alpha\cos\left(\frac{\phi}{2}\right)i_2 + \beta\sin\left(\frac{\phi}{2}\right)q_2\right)\right\}. \quad (3.3.6)$$

Several simplifications apply to equation (3.3.6). First, using the notation of Table 3.1, the expectations $E\{i_1 i_2\}$, $E\{q_1 q_2\}$, $E\{i_1 q_2\}$, and $E\{i_2 q_1\}$ can be replaced by $R_{ii}(\tau)$, $R_{qq}(\tau)$, $R_{iq}(\tau)$, and $R_{qi}(\tau)$, respectively. Secondly, the part of the expectations containing only one term in $i(t)$ or $q(t)$ are equal to zero due to the zero-mean assumption. Finally, the properties in equation (3.3.3) simplify the result. The final result is

$$Rq_{ii}(\tau) = \left(\alpha^2\sin^2\left(\frac{\phi}{2}\right) + \beta^2\cos^2\left(\frac{\phi}{2}\right)\right)R_{ii}(\tau). \quad (3.3.7)$$

Similarly, the following auto- and cross-correlation functions of the zero-mean quadrature modulator outputs are found:

$$\begin{aligned} Rq_{ii}(\tau) &= AR_{ii}(\tau) \\ Rq_{qq}(\tau) &= BR_{ii}(\tau) \\ Rq_{iq}(\tau) &= CR_{ii}(\tau) + DR_{iq}(\tau) \\ Rq_{qi}(\tau) &= CR_{ii}(\tau) - DR_{iq}(\tau) \end{aligned} \quad (3.3.8)$$

where

$$\begin{aligned} A &= \alpha^2\cos^2\left(\frac{\phi}{2}\right) + \beta^2\sin^2\left(\frac{\phi}{2}\right) \approx 1+\varepsilon \\ B &= \alpha^2\sin^2\left(\frac{\phi}{2}\right) + \beta^2\cos^2\left(\frac{\phi}{2}\right) \approx 1-\varepsilon \\ C &= \sin(\phi) \approx \phi \\ D &= \alpha\beta\cos(\phi) \approx 1 - \frac{\varepsilon^2+\phi^2}{2} \end{aligned} \quad (3.3.9)$$

For τ=0 the autocorrelation functions are:

$$Rq_{\ddot{u}}(0) = AR_{\ddot{u}}(0) = AR_m(0)$$

$$Rq_{qq}(0) = BR_{\ddot{u}}(0) = BR_m(0) \tag{3.3.10}$$

$$Rq_{iq}(0) = CR_{\ddot{u}}(0) = CR_m(0)$$

$$Rq_{qi}(0) = CR_{\ddot{u}}(0) = CR_m(0).$$

The DC part of the quadrature modulator output follows directly from equations (2.2.1) and (2.2.2). The offsets are

$$\mu_1 = a_1\alpha\cos\left(\frac{\phi}{2}\right) + a_2\beta\sin\left(\frac{\phi}{2}\right) \approx a_1 \tag{3.3.11}$$

$$\mu_2 = a_1\alpha\sin\left(\frac{\phi}{2}\right) + a_2\beta\cos\left(\frac{\phi}{2}\right) \approx a_2$$

3.3.3 Power Amplifier Autocorrelation

The amplifier output autocorrelation is defined as follows:

$$R_a(\tau) = \frac{1}{2}E\{V_a(t)V_a^*(t+\tau)\} \tag{3.3.12}$$

where $$V_a(t) = V_q(t)[\zeta_1 + \zeta_3|V_q(t)|^2], \tag{3.3.13}$$

$$V_a^*(t+\tau) = V_q^*(t+\tau)[\zeta_1^* + \zeta_3^*|V_q(t+\tau)|^2].$$

If we denote

$$V_q(t) = V_1 \tag{3.3.14}$$

and $$V_q(t+\tau) = V_2$$

then
$$\begin{aligned} 2R_a(\tau) = &\zeta_1\zeta_1^*E\{V_1V_2^*\} \\ &+ \zeta_1\zeta_3^*E\{V_1V_2V_2^{*2}\} \\ &+ \zeta_1^*\zeta_3E\{V_1^2V_1^*V_2^*\} \\ &+ \zeta_3\zeta_3^*E\{V_1^2V_1^*V_2V_2^{*2}\}. \end{aligned} \tag{3.3.15}$$

Each of the expectations above are now further expanded in terms of zero-mean jointly Gaussian random variables and scalars μ_1 and μ_2. In each expansion, V_1 and V_2 are replaced with

$$V_1 = (x_1 + \mu_1) + j(y_1 + \mu_2) \tag{3.3.16}$$

$$V_2 = (x_2 + \mu_1) + j(y_2 + \mu_2)$$

where x_1 and x_2 are the real and imaginary parts of the quadrature modulator output as defined in Table 3.1. The 2nd order expectation is given below.

$$\begin{aligned} E\{V_1 V_2^*\} &= E\{(x_1 + \mu_1 + j(y_1 + \mu_2))(x_2 + \mu_1 - j(y_2 + \mu_2))\} \\ &= E\{x_1 x_2 + \mu_1^2 + y_1 y_2 + \mu_2^2 + j y_2 x_1 + j\mu_1\mu_2 - j x_1 y_2 - j\mu_1\mu_2\} \\ &= Rq_{ii}(\tau) + Rq_{qq(\tau)} + jRq_{qi}(\tau) - jRq_{iq}(\tau) + \mu_1^2 + \mu_2^2 \\ &= (A + B)R_{ii}(\tau) - j2DR_{iq}(\tau) + \mu_1^2 + \mu_2^2 \\ &= 2R_{ii}(\tau) - j2DR_{iq}(\tau) + \mu_1^2 + \mu_2^2 \end{aligned} \tag{3.3.17}$$

As a first check, equation (3.3.17) is evaluated with no quadrature modulator errors. With no errors, $D = 1$, $\mu_1 = 0$, and $\mu_2 = 0$, giving

$$E\{V_1 V_2^*\}\,|_{noQMerrors} = 2R_{ii}(\tau) - j2R_{iq}(\tau) = 2R_m(\tau) \tag{3.3.18}$$

as expected.

The higher order expansions derived from equations (3.3.15) and (3.3.16) are very lengthy. In general, the expansions from equation (3.3.15) to forms containing x, y, and μ contain expectations of more than 2 jointly Gaussian zero-mean variables. These expansions were calculated using the following formula for mixed moments [19]:

$$E\{x_1 x_2 \ldots x_L\} = \begin{cases} 0 & \text{if } L \text{ is odd} \\ \sum\limits_{\substack{\text{all distinct pairs} \\ \text{of subscripts}}} (\lambda_{ij}\lambda_{lm}\ldots\lambda_{pL}) & \text{if } L \text{ is even} \end{cases} \tag{3.3.19}$$

where p=L-1, $\lambda_{ij} = E\{x_i x_j\}$, and where repeated subscripts are treated as distinct when applying the formula. For example, the second term of equation (3.3.15) expands to the following:

$$\begin{aligned} E\{V_1 V_2 V_2^{*2}\} =& E\{x_1 x_2^3 + x_1 x_2 y_2^2 + x_1 x_2(3\mu_1^2 + \mu_2^2) + 2x_1 y_2 \mu_1 \mu_2 + y_1 x_2^2 y_2 \\ & + 2y_1 x_2 \mu_1 \mu_2 + y_1 y_2^3 + y_1 y_2(\mu_1^2 + 3\mu_2^2) + x_2^2(3\mu_1^2 + \mu_2^2) \\ & + 4x_2 y_2 \mu_1 \mu_2 + y_2^2(\mu_1^2 + 3\mu_2^2) + \mu_1^4 + \mu_2^4 + 2\mu_1^2\mu_2^2\} \\ & + jE\{-x_1 x_2^2 y_2 - 2x_1 x_2 \mu_1 \mu_2 - x_1 y_2^3 - x_1 y_2(\mu_1^2 + 3\mu_2^2) + y_1 x_2^3 \\ & + y_1 x_2 y_2^2 + y_1 x_2(3\mu_1^2 + \mu_2^2) + 2y_1 y_2 \mu_1 \mu_2 + 2x_2^2 \mu_1 \mu_2 \\ & - 2x_2 y_2(\mu_1^2 - \mu_2^2) - 2y_2^2 \mu_1 \mu_2\}. \end{aligned} \tag{3.3.20}$$

The above equation can be further simplified to

$$\begin{aligned} E\{V_1 V_2 V_2^{*2}\} =& R_m(0) R_{ii}(\tau)[12 - 4AB + 4C^2] \\ & + [R_{ii}(\tau) + R_m(0)][2\mu_1^2(1 + A) + 2\mu_2^2(1 + B) + 4\mu_1\mu_2 C] \\ & + (\mu_1^2 + \mu_2^2)^2 \\ & + j\{R_m(0) R_{iq}(\tau)[-8D] \\ & + [R_{ii}(\tau) - R_m(0)][2C(\mu_1^2 - \mu_2^2) - 2\mu_1\mu_2(A - B)] \\ & + R_{iq}(\tau)[-4D(\mu_1^2 + \mu_2^2)]\} \end{aligned} \tag{3.3.21}$$

where A, B, C, D, and μ are as defined in equation (3.3.9) and (3.3.11).

The simplification of the third term of equation (3.3.15) is similar to (3.3.21) in length and content, and the fourth term is roughly twice as complex. These results, while interesting, are not very useful or enlightening, and are given in Appendix B. One further assumption does give tractable results, though. If one assumes a symmetric spectrum, then $R_{iq}(\tau)$ becomes zero and the output autocorrelation becomes much simpler:

$$R_a(\tau) \approx P_0 + P_1 R_m(\tau) + P_2 R_m^2(\tau) + P_3 R_m^3(\tau) \tag{3.3.22}$$

where

$$
\begin{aligned}
P_0 &= |\zeta_1|^2\left(\frac{\mu_1^2+\mu_2^2}{2}\right)+Re(\zeta_1\zeta_3^*)(\mu_1^2+\mu_2^2)^2 \\
&\quad +2Re(\zeta_1\zeta_3^*)R_m(0)(\mu_1^2(2+\varepsilon)+\mu_2^2(2-\varepsilon)+2\mu_1\mu_2\phi) \\
&\quad -2Im(\zeta_1\zeta_3^*)R_m(0)[\phi(\mu_1^2-\mu_2^2)-2\mu_1\mu_2\varepsilon] \\
&\quad +|\zeta_3|^2R_m(0)^2[2(2+\varepsilon)^2\mu_1^2+2(2-\varepsilon)^2\mu_2^2+16\mu_1\mu_2\phi] \\
&\quad +|\zeta_3|^2R_m(0)[4(\mu_1^4+\mu_2^4)+8\mu_1^2\mu_2^2+2\varepsilon(\mu_1^4-\mu_2^4)] \\
&\quad +|\zeta_3|^2R_m(0)[4\mu_1\mu_2(\mu_1^2+\mu_2^2)\phi] \\
&\quad +|\zeta_3|^2\frac{1}{2}(\mu_1^2+\mu_2^2)^3, \\
P_1 &= |\zeta_1|^2+2Re(\zeta_1\zeta_3^*)R_m(0)[4+2\varepsilon^2\phi^2)] \\
&\quad +2Re(\zeta_1\zeta_3^*)[2(a_1^2+a_2^2)+\varepsilon(a_1^2-a_2^2)+2a_1a_2\phi] \\
&\quad +2Im(\zeta_1\zeta_3^*)[\phi(a_1^2-a_2^2)-2a_1a_2\varepsilon] \\
&\quad +|\zeta_3|^2R_m(0)^2[16+20\varepsilon^2+4\phi^2-2\varepsilon^2\phi^2-2\phi^4] \\
&\quad +|\zeta_3|^2R_m(0)[(a_1^2+a_2^2)(16+8(\varepsilon^2+\phi^2))+12\varepsilon(a_1^2-a_2^2)] \\
&\quad +|\zeta_3|^2[5(a_1^4+a_2^4)+4\varepsilon(a_1^4-a_2^4)+10a_1^2a_2^2+8a_1a_2(a_1^2+a_2^2)\phi], \\
P_2 &= |\zeta_3|^2[(a_1^2+a_2^2)(12+16\phi^2+8\varepsilon^2)+16\varepsilon(a_1^2-a_2^2)+32a_1a_2\phi], \\
P_3 &= |\zeta_3|^2[8+16(\varepsilon^2+\phi^2)]
\end{aligned}
\tag{3.3.23}
$$

and the approximations of equations (3.3.9) and (3.3.11) have been used to obtain (3.3.23). The spectral results corresponding to equation (3.3.22) is given in the next section.

3.3.4 Power Amplifier Spectrum

The power spectral density of the amplifier output is related to the autocorrelation function by the Fourier transform, that is

$$S_a(w) = \int_{-\infty}^{+\infty} R_a(\tau) e^{-jw\tau} d\tau \tag{3.3.24}$$

or

$$S_a(w) = \mathcal{FT}\,[R_a(\tau)]$$

Two properties of the Fourier transform are needed to obtain the final result. These are the linearity and the frequency convolution properties:

linearity

$$\begin{aligned} &\textit{If} \quad \mathcal{FT}\,[g(\tau)] = G(w) \\ &\textit{and} \quad \mathcal{FT}\,[h(\tau)] = H(w), \\ &\textit{then} \quad \mathcal{FT}\,[a\,g(\tau) + b\,h(\tau)] = aG(w) + bH(w) \end{aligned} \tag{3.3.25}$$

frequency convolution

$$\begin{aligned} &\textit{If} \quad \mathcal{FT}\,[g(\tau)] = G(w) \\ &\textit{and} \quad \mathcal{FT}\,[h(\tau)] = H(w) \\ &\textit{then} \quad \mathcal{FT}\,[g(\tau)h(\tau)] = \frac{1}{2\pi} G(w) \otimes H(w) \end{aligned} \tag{3.3.26}$$

where $\otimes$ represents convolution. Using equation (3.3.25), the parts of (3.3.22) are separated into four parts so that (3.3.24) becomes

$$S_a(w) = \mathcal{FT}\,[P_0] + P_1 \mathcal{FT}\,[R_m(\tau)] + P_2 \mathcal{FT}\,[R_m^2(\tau)] + P_3 \mathcal{FT}\,[R_m^3(\tau)]. \tag{3.3.27}$$

Then, using the convolution property (equation (3.3.26)

$$\begin{aligned} S_a(w) = 2\pi P_0 \delta(w) + P_1 S_m(w) + \frac{1}{2\pi} P_2 S_m(w) \otimes S_m(w) \\ + \frac{1}{4\pi^2} S_m(w) \otimes S_m(w) \otimes S_m(w) \end{aligned} \tag{3.3.28}$$

where $S_m(w)$ is the Fourier transform of $R_m(\tau)$, that is $S_m(w)$ is the spectrum of the input signal.

Equation (3.3.28) is an important result. If $S_m(w)$ has a bandwidth BW, then $S_m(w) \otimes S_m(w)$ has a bandwidth 2BW, and $S_m(w) \otimes S_m(w) \otimes S_m(w)$ has a bandwidth 3BW. These two terms thus represent a spreading of the input spectrum into adjacent

frequencies. Furthermore, from equation (3.3.23) it is clear that P_2 is a quadratic function of DC offset error, and P_3 is a quadratic function of gain imbalance and phase error. Also, both P_2 and P_3 are quadratic in power amplifier nonlinearity, ζ_3.

Therefore, for a zero-mean, WSS Gaussian random input signal with symmetric spectrum (I and Q channels independent), the adjacent channel power is individually quadratic in power amplifier nonlinearity and quadrature modulator errors.

3.4 Summary of Analysis Results

Two different input signals have been used to obtain the same analytical result: Adjacent channel power is a quadratic function of power amplifier nonlinearity (third order model), and also of quadrature modulator errors.

The quadratic result is important in terms of automatic adjustment of the system. Since the adjacent channel power surface is quadratic, we know that just a single minimum exists, and thus whatever the optimization method we choose, we should not have problems with false (local) minima. Also, the quadratic shape lends itself to surface-fit optimization methods as the next section describes.

4 ADAPTATION ALGORITHM

The analysis of Section 3 showed that adjacent channel power was a quadratic function of power amplifier nonlinearity (or predistorter mis-adjustment), and also of quadrature modulator error (or quadrature modulator compensator mis-adjustment). In this section, a new surface fit technique is described which uses the predicted power surface to achieve good convergence rates. The method uses a recursive least-squared-error (RLS) approach to fit a set of measured data onto a power surface. From the estimated power surface an optimum set of coefficients is calculated.

The basic algorithm was conceived by Jim Cavers [20].

4.1 General Description

A quadratic power surface can be expressed as a function $f(x)$ given by

$$f(x) = Re(x^{*T} H x + g^{*T} x + C) \tag{4.1.1}$$

where x specifies the set of (complex) coefficients,

H is a Hessian matrix [16],

g is the gradient of x at x=0,

C is the function evaluation at x=0.

As an example, the quadrature modulator coefficients a_1, a_2, ε, and φ could form the following x:

$$x = \begin{pmatrix} a_1 + j a_2 \\ \varepsilon + j\phi \end{pmatrix} = \begin{pmatrix} x_0 \\ x_1 \end{pmatrix} \tag{4.1.2}$$

In such a system, H is a real 2x2 matrix, g is a complex vector of length 2, and C is a real number. $f(x)$ has a minimum at $x = x_{opt}$ given by

$$x_{opt} = -\frac{1}{2} H^{-1} g \tag{4.1.3}$$

Unfortunately, we don't know H or g a priori and thus finding x_{opt} depends on our ability to determine H and g. As the next section shows, the RLS method can be applied to determine H, g, and C.

4.2 Adaptation by Recursive Least-Squared-Error Fit

With the least-squared-error (LSE) method, measured data points are fit to the surface such that the sum of squared errors is minimized: Errors are the distances from the measured and fitted surface. A recursive LSE method (RLS) is similar to the LSE method except that *all* data points are used and more recently measured points can be given a greater weighting in the surface fit. (The weighted fit allows the algorithm to follow time-variant signals or systems.)

In applying the RLS algorithm, $f(x)$ is first expressed as the product of two vectors. Expanding equation (4.1.1) and rewriting gives

$$f(x) = p^T \cdot a(x) \tag{4.2.1}$$

where

$$p = \begin{pmatrix} H_{0,0} \\ H_{0,1} \\ H_{1,1} \\ Re(g_0) \\ Im(g_0) \\ Re(g_1) \\ Im(g_1) \\ C \end{pmatrix}, \qquad a(x) = \begin{pmatrix} |x_0|^2 \\ 2Re(x_0 x_1^*) \\ |x_0|^2 \\ Re(x_0) \\ Im(x_0) \\ Re(x_1) \\ Im(x_1) \\ 1 \end{pmatrix} \tag{4.2.2}$$

The error for each measured point is given by

$$e(i) = f(x(i)) - m(i) \tag{4.2.3}$$

where $x(i)$ is the i^{th} point measured and $m(i)$ is the power measurement of the i^{th} point.

Next, define

$$
\begin{aligned}
V(k) &= \sum_{i=0}^{k} \lambda^{k-i} e(i)^2 \\
&= \sum_{i=0}^{k} \lambda^{k-i} (f(x(i)) - m(i))^2 \\
&= \sum_{i=0}^{k} \lambda^{k-i} (a(x(i))^T \cdot p - m(i))^2 \\
&= \sum_{i=0}^{k} \lambda^{k-i} [a(x(i))^T \cdot a(x(i)) \cdot p^T \cdot p - 2a(x(i))^T \cdot p \cdot m(i) + m(i)^2]
\end{aligned}
\tag{4.2.4}
$$

where a total of k measurements are available and λ is typically set to just less than one to favour more recent measurements. To determine the optimum set of coefficients of H and g, we take the derivative of $V(k)$ with respect to p:

$$
\frac{d(V(k))}{dp} = \sum_{i=0}^{k} \lambda^{k-i} 2[a(x(i))^T \cdot a(x(i)) \cdot p - m(i) \cdot a(x(i))]. \tag{4.2.5}
$$

Setting equation (4.2.5) to zero yields the optimum coefficients, and the following relationship:

$$
\sum_{i=0}^{k} \lambda^{k-i} a(x(i))^T \cdot a(x(i)) \cdot p = \sum_{i=0}^{k} \lambda^{k-i} m(i) \cdot a(x(i)). \tag{4.2.6}
$$

Defining

$$
\begin{aligned}
R(k) &= \sum_{i=0}^{k} \lambda^{k-i} a(x(i)) \cdot a(x(i))^T, \\
W(k) &= \sum_{i=0}^{k} \lambda^{k-i} m(i) \cdot a(x(i)),
\end{aligned}
\tag{4.2.7}
$$

substituting into equation (4.2 6), and re-arranging gives

$$
p = R^{-1}(k) \cdot W(k) \tag{4.2.8}
$$

At this point we note that both $R(k)$ and $W(k)$ can be calculated recursively.

$$
\begin{aligned}
W(k) &= \lambda W(k-1) + m(k) a(x(k)) \\
R(k) &= \lambda R(k-1) + a(x(k)) a(x(k))^T
\end{aligned}
\tag{4.2.9}
$$

As new points are measured, $W(k)$ and $R(k)$ are calculated from which p is computed. In turn, p gives an updated optimum set of H, g, and C, and hence a new x_{opt} can be found.

This formulation of the surface fit algorithm is much like an adaptive FIR filter [21] where p is the filter coefficient vector, a is the input signal vector, and m is the desired sequence.

The RLS method should be much faster than the gradient or the direct-search methods. However, computationally it is somewhat more complex. Another disadvantage of the RLS algorithm is its sensitivity to round-off errors that accumulate as a result of the recursive computations. Experimentally, Proakis [21] reports that approximately 24 bits of precision are needed for the RLS algorithm to work properly. However, for short bursts (less than 500 iterations) as little as eleven bits may be sufficient.

4.3 Efficient Algorithm Calculations

The basic RLS algorithm is computationally intensive, requiring the inversion of two matrices (H and R) and several vector multiplications. This section addresses methods which reduce the computational needs of the algorithm.

The most intensive operation in the RLS algorithm is the inversion of the R matrix. Even for two (complex) variable optimization, we get an R matrix which is 8x8 (real). Fortunately, the matrix inversion lemma [22] allows us to calculate R^{-1} recursively, instead of R. Letting $S(k) = R^{-1}(k)$, the matrix inversion lemma gives the following recursion formula:

$$S(k) = \lambda^{-1} \cdot S(k-1) - \lambda^{-2} \cdot \frac{r(k-1) \cdot r(k-1)^T}{1 + \lambda^{-1} \cdot a(x(k-1))^T \cdot r(k-1)} \tag{4.3.1}$$

where $r(k) = S(k) \cdot a(x(k))$. For S of size $n \times n$, calculation of $S(k)$ requires approximately $2n^2$ real additions and multiplications. Using the Kalman gain factor [21], the complexity can be reduced to approximately $7n$ multiplications.

Another area of improvement is in the initial start-up of the algorithm. The initial S matrix is often set to δI, where δ is a small positive number and I is the identity matrix. A better option is to use a set of n test vector to purposely explore the power surface. At start-up, if the same n outputs are used, it is possible to pre-calculate S and store it in memory for later use. (Equation (4.2.7) shows that R and hence S are uniquely determined by the test vectors only, not the measured values). A set of vectors which give orthogonal a vectors are

$$x_0 = \begin{pmatrix} 1.5 + j0.5 \\ 0.5 + j0.0 \end{pmatrix} \quad x_1 = \begin{pmatrix} -0.5 - j0.5 \\ 1.0 - j1.0 \end{pmatrix} \quad x_2 = \begin{pmatrix} -1.0 + j1.0 \\ -1.5 + j0.0 \end{pmatrix}$$

$$x_3 = \begin{pmatrix} 1.0 + j0.0 \\ -1.0 - j0.5 \end{pmatrix} \quad x_4 = \begin{pmatrix} -1.5 - j1.0 \\ 0.0 + j0.5 \end{pmatrix} \quad x_5 = \begin{pmatrix} 0.5 - j1.5 \\ 0.0 + j1.0 \end{pmatrix} \tag{4.3.2}$$

$$x_6 = \begin{pmatrix} 0.0 + j0.0 \\ -0.5 + j1.5 \end{pmatrix} \quad x_7 = \begin{pmatrix} 0.0 + j1.5 \\ 0.0 - j1.5 \end{pmatrix}$$

For the above test vectors, the initial S matrix is (4.3.3)

$$S = \begin{pmatrix} 0.4883 & 0.07985 & 0.6344 & 0.2741 & -0.3251 & 0.03213 & -0.08774 & -1.72 \\ 0.07985 & 0.04546 & 0.1228 & 0.06558 & -0.09845 & -3.872 \cdot 10^{-6} & -0.05541 & -0.286 \\ 0.6344 & 0.1228 & 1.089 & 0.4315 & -0.5651 & 0.06624 & -0.1524 & -2.605 \\ 0.2741 & 0.06558 & 0.4315 & 0.3347 & -0.2832 & -0.02806 & -0.1055 & -1.069 \\ -0.3251 & -0.09845 & -0.5651 & -0.2832 & 0.6218 & 0.1451 & 0.3063 & 1.352 \\ 0.03213 & -3.872 \cdot 10^{-6} & 0.06624 & -0.02806 & 0.1451 & 0.3477 & 0.1506 & -0.08834 \\ -0.08774 & -0.05541 & -0.1524 & -0.1055 & 0.3063 & 0.1506 & 0.3361 & 0.3641 \\ -1.72 & -0.286 & -2.605 & -1.069 & 1.352 & -0.08834 & 0.3641 & 6.73 \end{pmatrix}.$$

Finally, there is the question of number of variables. In the desired system, we have two complex predistorter coefficients (5^{th} order predistortion) and 4 real quadrature modulator compensator coefficients for a total of 8 real variables. As previously stated, for two complex (or four real) variable optimization, a, p, and W are length 8 vectors, and R or S is 8x8. For four complex (or eight real) variable optimization, a, p, and W turn out to be 19x1, with S having 19 rows and columns. As well, four complex variables imply that H is 4x4, as compared to the two variable case when H is 2x2. Since the matrix inversion lemma cannot be applied to H, the two variable optimization is simpler in this respect.

The last element compelling us to separate the algorithm into two two-variable optimizations is the adjacent channel power function itself. The adjacent channel power is individually quadratic in either predistorter or quadrature modulator error, but of fourth order when considered as a function of both PD and QM together (equations (3.3.23) and (3.3.28)). Therefore, the quadratic assumption is only justified in the separate optimization case.

The final solution uses two sets of two complex variable optimization, one for the predistorter and one for the quadrature modulator. After a limited number of iterations, the algorithm switches from one set of variables to the next. This solution is computationally simple due to the reduced dimensions of the matrices, avoids round-off errors, and the power surfaces are true quadratic shapes.

Sections 5 and 6 report on the simulated and implemented performance of the algorithm.

5 SIMULATION

The analysis of Section 3 showed that adjacent channel power was a quadratic function of power amplifier and quadrature modulator error, or equivalently, of predistorter and quadrature modulator compensator mis-adjustment. The analysis was for tone and WSS Gaussian inputs, however, which are somewhat different from real data signals. This section presents simulation results which verify the analysis, only with a real data signal using offset quadrature phase-shift keyed (offset QPSK) modulation. Also, simulation results for the optimization method described in the previous section are given.

5.1 Simulation Model

The simulation model was designed to match the implemented system as closely as possible. Figure 5.1 illustrates the model.

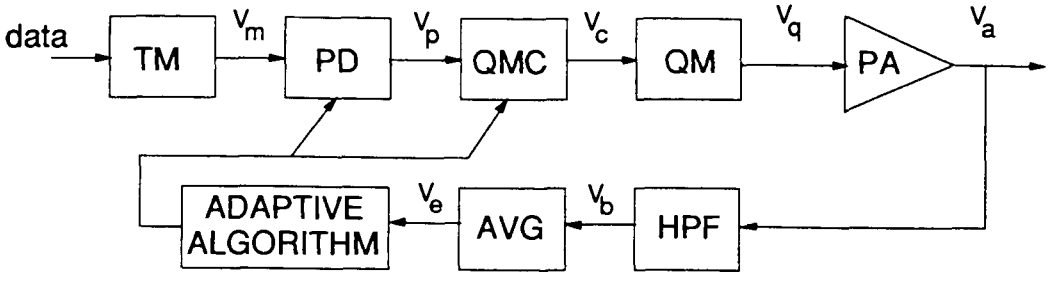

Figure 5.1 Simulation Model

The simulation was performed on a Sun Sparc computer system and was programmed in the 'C' language.

5.1.1 Transmit Modem

Offset QPSK modulation was used in the simulation. Offset QPSK is like QPSK, except that the quadrature channel output is delayed by one-half a bit-time. The advan-

tage of offset QPSK over QPSK is its reduced dynamic range: offset QPSK's signal power never approaches zero.

Mathematically, the offset QPSK output is expressed as

$$V_m(t) = \sum_{k=-\infty}^{\infty} \left(a_k p(t - kT) + j b_k p\left(t - kT - \frac{T}{2} \right) \right) \tag{5.1.1}$$

where T is the symbol period, $p(t)$ is the pulse shape, and a_k and b_k are ±1 depending on the input data bits. A raised-cosine pulse shape was used. This pulse shape is defined as

$$p(t) = \frac{\pi}{4} \text{sinc}(t) \left(\text{sinc}\left(\beta t + \frac{1}{2} \right) + \text{sinc}\left(\beta t - \frac{1}{2} \right) \right) \tag{5.1.2}$$

where the sinc(x) function is defined as $\sin(x)/x$, and a rolloff factor β of 0.33 was used. The pulse was truncated to 8 symbols in length and sampled at 16 samples per symbol, and the resulting sequence was Kaiser windowed with Kaiser parameter 4 [23].

5.1.2 Predistorter

The predistorter is a 5th order polynomial predistorter as illustrated in Figure 2.4 on page 13. The predistorter gain is given by $F(X_m)$:

$$F(X_m) = \kappa_1 + \kappa_3 X_m + \kappa_5 X_m^2 \tag{5.1.3}$$

where X_m is the input power to the predistorter. In the simulation κ_1 was initialized to

$$\kappa_1 = 0.58315 - j0.00395 \tag{5.1.4}$$

to get a first-order match with the power amplifier. The complex κ_3 and κ_5 coefficients were then adjusted.

5.1.3 Quadrature Modulator and Compensator

The quadrature modulator is the symmetric model described in Section 2.2.1 and modelled with equations (2.2.1) and (2.2.2). The quadrature modulator errors were fixed at 5 percent gain imbalance, −0.05 radian phase error, and 5 percent DC offsets errors

(relative to the peak pulse amplitude).

The quadrature modulator compensator is the symmetric one described in Section 2.2.2 and modelled with equations (2.2.4) and (2.2.5). The quadrature modulator compensator's parameters (gain, phase, and DC offset errors) were adjustable.

5.1.4 Power Amplifier

The power amplifier characteristic was based on the measured characteristics of a class AB, 5 Watt amplifier from 3dbm [24]. The characteristic complex gain of the amplifier is shown below. The simulation uses the data shown in the graph to simulate the power amplifier.

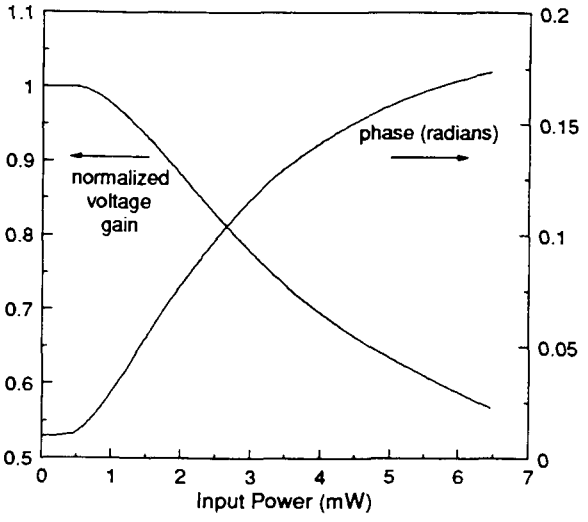

Figure 5.2 Complex Gain of Class AB Amplifier

5.1.5 Power Detector

The power detector consists of an IIR filter and averager. The IIR filter was an 8th order elliptic highpass filter with cutoff at 0.065 (f/f_s), where f_s is the sampling frequency. The filter provides a stopband attenuation of greater than 84 dB from 0 to 0.05 (f/f_s) and passband ripple of 1 dB. The cutoff frequency is equivalent to 12.5 kHz for a system with

12.5 k-symbol per second modulation rate, with the stopband extending to 10 kHz. Figure 5.3 shows the frequency response of the filter which was designed using DFDP [25] (Digital Filter Design Program).

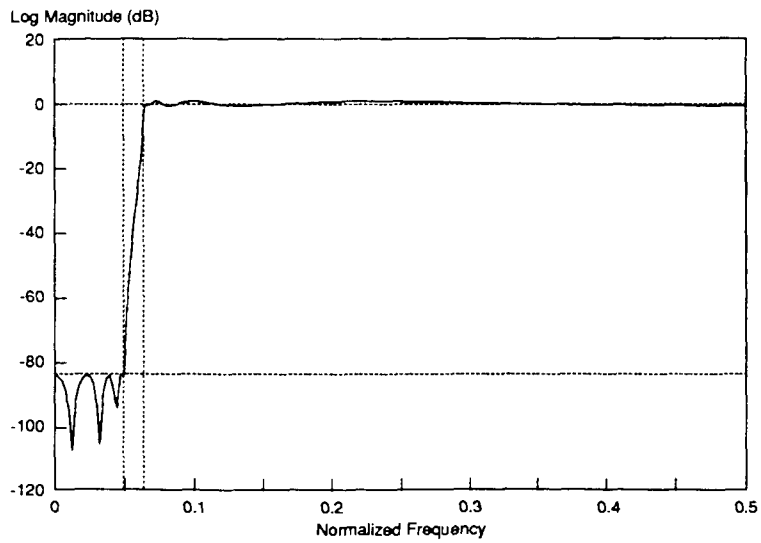

Figure 5.3 Power Detector Filter Frequency Response

The detector works as follows. The in-phase and quadrature signals are fed through separate filters, and the square of each filter output sample is calculated, summed, and added to a running total. The power is normalized by dividing by the number of symbols in each measurement, usually between 500 and 10,000.

5.2 Adjacent Channel Power Dependence on Coefficients

Figures 5.4 and 5.5 show the adjacent channel power versus predistorter and quadrature modulator compensator coefficients. In the simulation, 5000 symbols were used for each power measurement, and coefficients not graphed were set to their optimum values.

The figures show the predicted quadratic shape of adjacent channel power for all

eight variables, including the fifth order predistorter coefficients which were not part of the analysis. The figures show that mis-adjustment of the fifth order coefficients gives the highest increase in adjacent channel power, followed by the third order coefficients, and then the quadrature modulator DC offset errors, phase error, and finally, the gain imbalance.

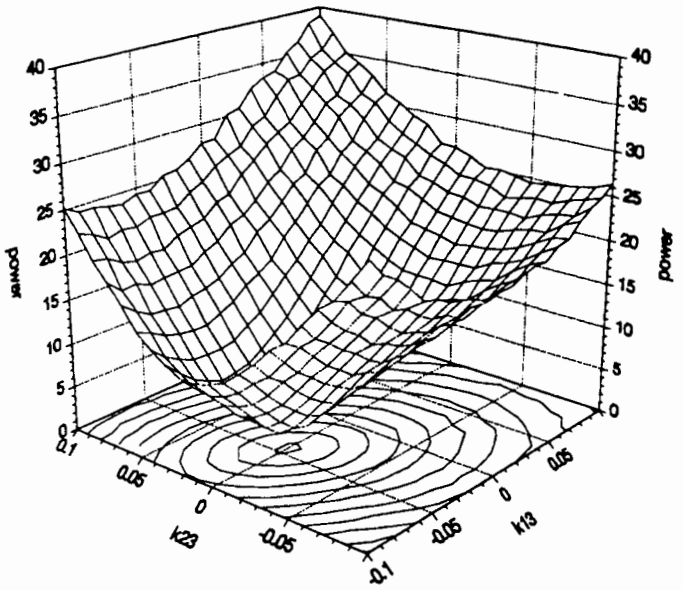

(a) third order coefficients

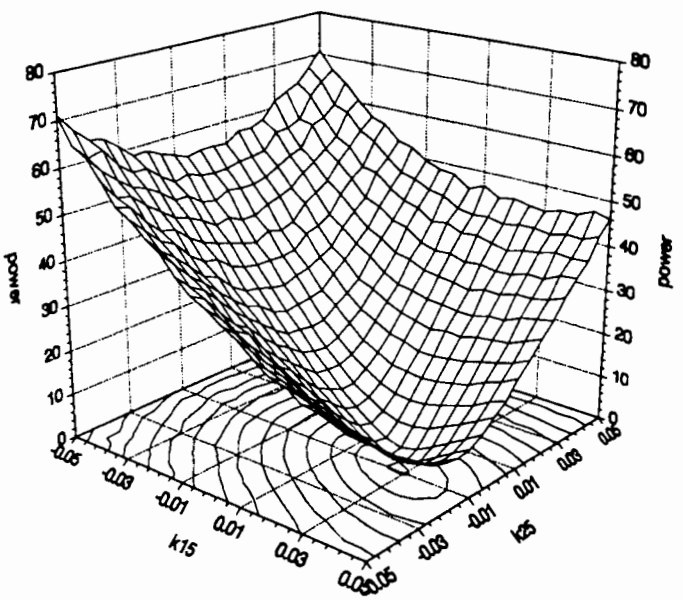

(b) fifth order coefficients

Figure 5.4 Simulated Adjacent Channel Power vs Predistorter Coefficients

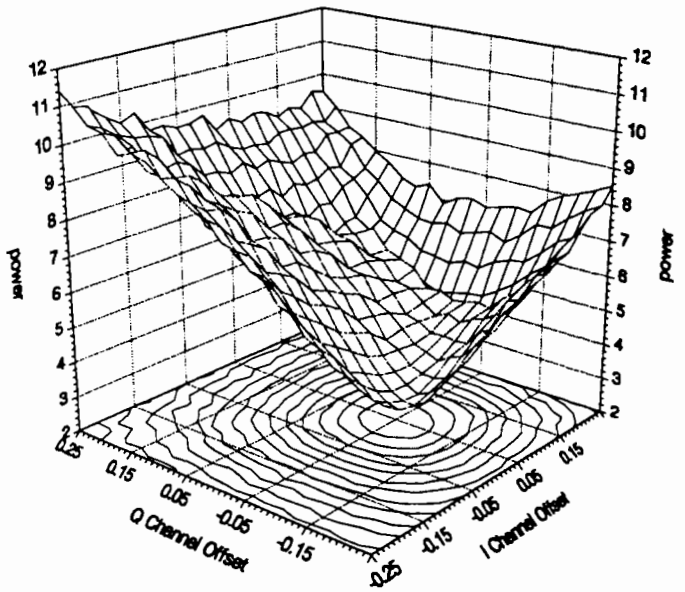

(a) DC voltage offset coefficients

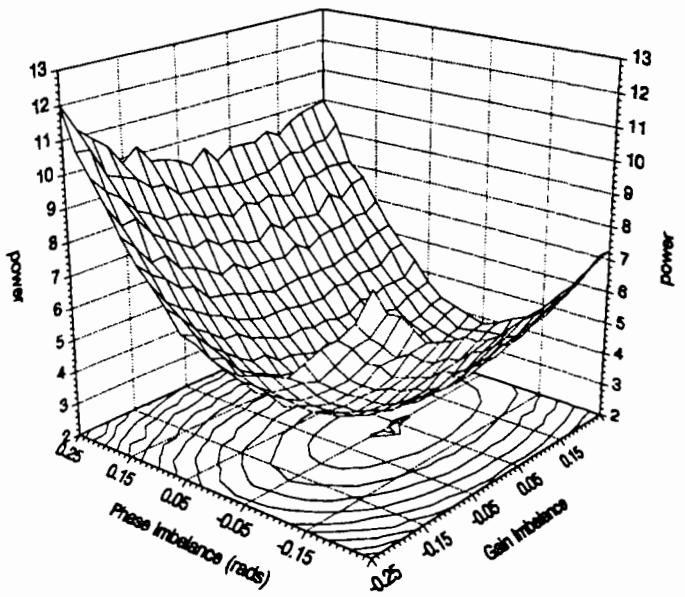

(b) gain and phase coefficients

Figure 5.5 Simulated Adjacent Channel Power vs Quadrature Modulator Compensator Coefficients

5.3 Adaptation of Coefficients - Recursive Least Squares Algorithm

The RLS algorithm discussed in Section 4 was simulated. As stated, the optimization is in fact two sets of 2 complex variable optimization, and thus the algorithm alternates between two sets of coefficients: one for the predistorter and one for the quadrature modulator compensator.

Each time the algorithm alternated, the coefficients were re-initialized to their previous optimum values, and this set of coefficients was perturbed with test vectors to explore the power surface. Even though the test vectors were scaled and offsets were added, the initial S matrix could still be used. After several measurements and least-squares calculations the algorithm alternated again between the predistorter and quadrature modulator compensator coefficients. With each coefficient switch, the scale of the test vectors was reduced to allow more precise adjustment of the coefficients and prevent large distortions of the data signal.

The algorithm was modified to allow the selection of a test vector if the test vector gave an adjacent channel power measurement which was significantly lower than the surface fit solution; this could occur when a noisy measurement disturbed the surface fit, or where the surface did not fit the quadratic assumption very well.

Experimentally it was found that the algorithm worked best if the number of iterations per individual optimization was limited to about 12, and that power measurements averaged over 500 symbol times was adequate.

The results of the optimization are shown in the next two figures. In Figure 5.6, the input spectrum and output spectrum (before optimization and after) are shown. The frequency axis is shown for a symbol rate of 12.5 kHz. A 20 dB reduction in adjacent channel power is recorded.

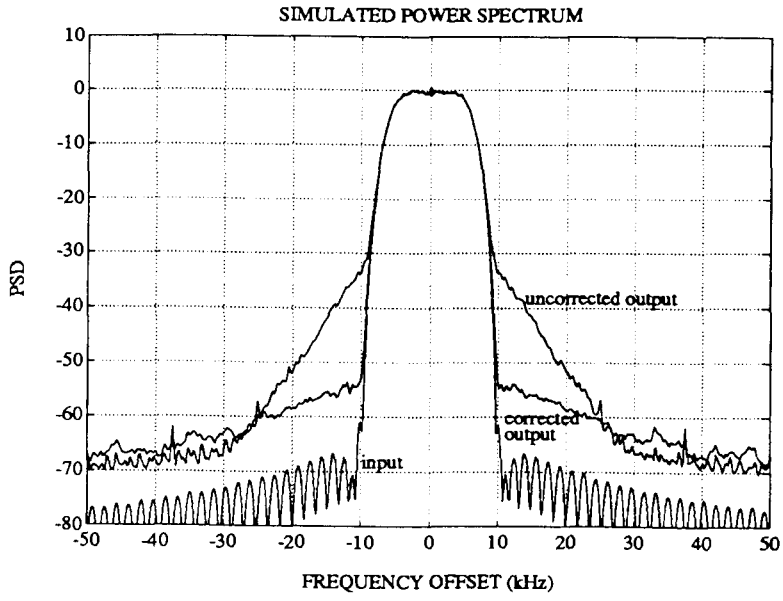

Figure 5.6 Spectrum Improvement with Predistortion and QMC

Figure 5.7 shows the speed of the algorithm. The simulation was run using 500 symbols per measurement, the number of iterations per individual optimization was limited to about 12, and the coefficients converged in approximately 3 seconds at a symbol rate of 12.5 kHz.

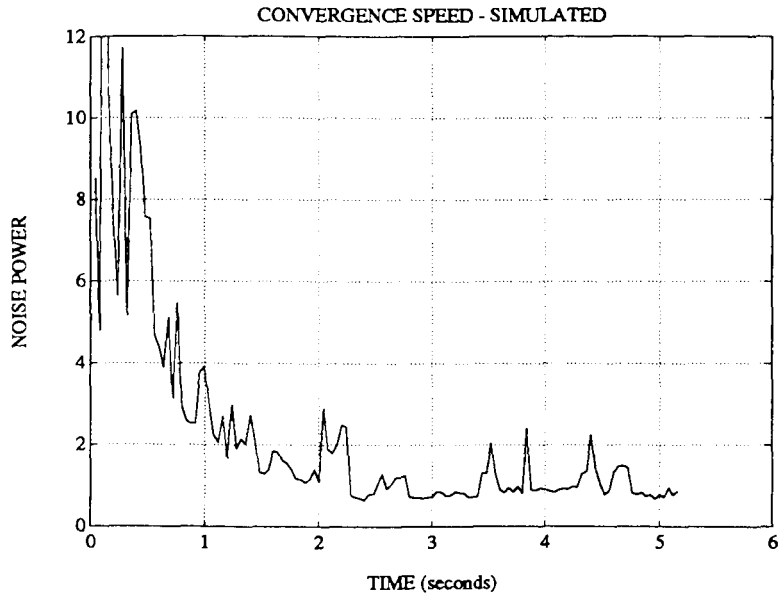

Figure 5.7 RLS Algorithm Speed

The simulated system performed very well, giving fast convergence and up to a 20 dB reduction in adjacent channel power. Sections 6 and 7 report on the actual system, its construction, and its performance.

6 IMPLEMENTATION

This section describes the hardware system used to verify the analytical and simulation results. An overview of the adaptive transmitter design is given, followed with detailed design information. Section 7 present the measured results. All hardware schematics are given in Appendix A.

6.1 System Overview

The hardware block diagram is shown below in Figure 6.1. The system is relatively simple thanks to a TMS320C25 [26] Digital Signal Processor (or simply the 'C25). A 'C25 system board from Spectrum Signal Processing Inc. [27] acts as a transmit modem, predistorter and quadrature modulator compensator. The digital output from the 'C25 is converted, via two digital-to-analog converters (DACs) and lowpass filters, to a continuous-time, analog signal. From here, a Hewlett-Packard quadrature modulator up-converts the baseband signal to 850 MHz.

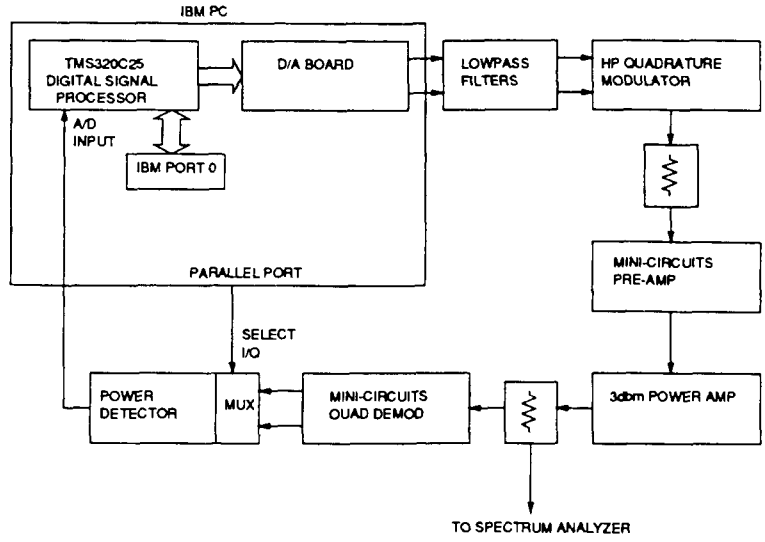

Figure 6.1 Hardware Overview

A Mini-Circuits [28] pre-amplifier drives the power amplifier – a class AB amp from 3dbm. The power amplifier output would normally feed to an antenna, but for testing purposes it is coupled to a spectrum analyzer. Some of the power amplifier output is coupled off to be down-converted with a quadrature demodulator built from standard Mini-Circuits mixers, combiners, and filters. The I/Q channels from the quadrature demodulator are multiplexed to a single power detector, and the detector output is 'read' by an analog-to-digital converter (ADC) on the 'C25 board. Control over the DSP board and power detector multiplexer are provided by the host AT computer using a shared PC-DSP port and the parallel port, respectively. The AT runs a 'C' program.

6.2 DSP Circuit

The DSP circuit reads in a bit stream, generates an offset QPSK signal, predistorts the signal, compensates for quadrature modulator error, and finally writes the complex baseband output to a pair of DACs. The software for the DSP is written in TMS320C25 assembler.

The following three section describe the DSP's operation.

6.2.1 Transmit Modem

The transmit modem takes pairs of random bits (generated by a HP 1645A Data Error Analyzer [6]) and produces the complex baseband signal defined by

$$V_m(t) = \sum_{k=-\infty}^{\infty} \left(a_k p(t - kT) + j b_k p\left(t - kT - \frac{T}{2} \right) \right) \tag{6.2.1}$$

where a_k and b_k are ± 1 depending on the input data bits, and $p(t)$ is the raise-cosine pulse shape.

The pulse $p(t)$ is limited to eight symbols in duration and is sampled at ten samples per symbol. The resulting sequence windowed with a Kaiser window, parameter 4. This

pulse is defined in Section 5.1.1, and a rolloff value of 33% was used. The symbol rate was 12,500 symbols per second giving a sample rate of 125 kHz.

Equation (6.2.1) is rather slow to implement directly in DSP, and so a table look-up method was used. The table method uses the fact that for each symbol output there are 2^8 possible combinations due to overlap of the consecutive eight pulses. The table look-up method pre-calculates and stores the 2^8 sequences for each output and thus requires only a simple indexing into the table. For ten samples/symbol and a pulse eight symbols long, there are $10x2^8$ words of storage, or 2560 words. With the table look-up method, the offset QPSK signal is generated using only about 20 instruction cycles for every symbol (10 complex samples), or about 0.2 μs per sample.

6.2.2 Predistorter

The next block in DSP takes the modem output and passes it through a 5^{th} order polynomial predistorter. Like Figure 2.4 on page 13, the predistorter is split into two blocks. The first generates the complex gain $F = F_1 + jF_2$, and the second generates the output signal, $V_p(t)$. Using the 'C25, the calculation of each complex sample takes 35 instruction cycles, or about 3.5 μs per sample.

6.2.3 Quad Mod Compensator

The output from the predistorter is then modified to compensate for quadrature modulator errors. The compensator uses the asymmetric model given in Section 2.2.2 since this model is simpler to implement than the symmetric one. The compensator calculations take only 11 instruction cycles, or about 1.1 μs per sample.

6.3 Lowpass Filters

The digital output from the TMS320C25 is converted to analog using two Burr-Brown [29] PCM53 DACs. Lowpass filters were used to prevent the frequency aliasing

which occurs with discrete-time signals. The filters were 6th order Butterworth filters designed using [30]. The simulated response of the filters is shown in Figure 6.2 below. The measured response of the filters was very close to the simulated, and the filters had less than 0.1 dB ripple in the passband.

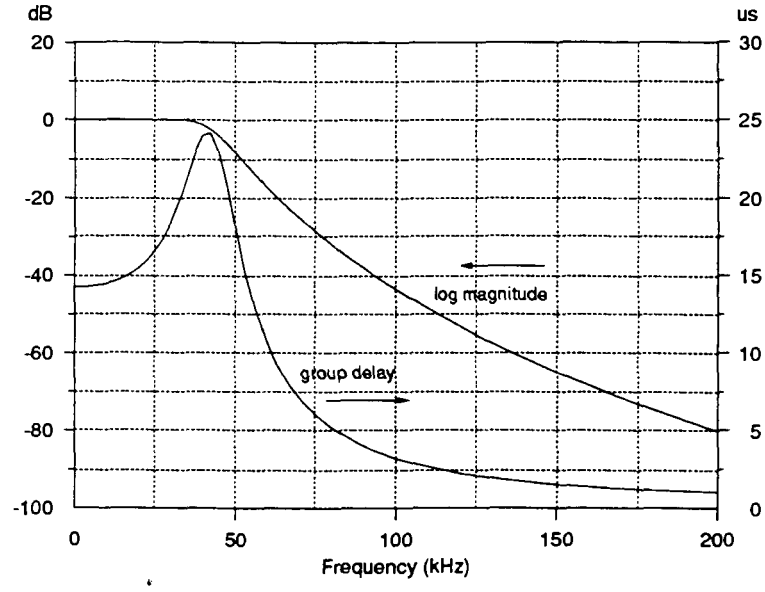

Figure 6.2 Lowpass Filter Response

6.4 Quadrature Modulator

The quadrature modulator was constructed from the recently released Hewlett-Packard chip, the HPMX-2001, by Sirooj Rambaran (SFU, 1992). The HPMX-2001 is a silicon based bipolar monolithic quadrature phase shift keyed modulator in a plastic 16 pin package. The chip is suitable for narrowband applications and has a typical LO operating frequency range of DC-2000 MHz. The chip has a low current drain of about 20 mA, and a saturated output power of -5.5 dBm into a 50 ohm load. The quadrature modulator schematic based on the HPMX-2001 is shown in Appendix A, and the DC offset, gain, and phase characteristics are shown in Figure 2.3 on page 7.

6.5 Quadrature Demodulator

Mini-Circuits parts were used to build the quadrature demodulator. The demodulator was designed and built by Sirooj Rambaran (SFU, 1992). The following parts were used:

mixers	SRA-2CM
0° power splitter	PSC-2-4
lowpass filters	PLP-10-7

An additional 90° power splitter was custom designed by S. Rambaran.

6.6 Adjacent Channel Power Detector

The power detector provides the feedback signal needed for the adaptive signal. The detector consists of four main parts: a multiplexer, two bandpass filters, and a Signetics [31] NE604 receiver chip. The detector block diagram is illustrated below (Figure 6.3), and is similar to an application suggested by Signetics [32].

The NE604 chip provides up to 90 dB gain and also a 'received-signal-strength-indicator', or RSSI. The RSSI voltage is proportional to the signal strength in decibels and gives the required adjacent channel power signal. The complete power detector schematic is shown in Appendix A.

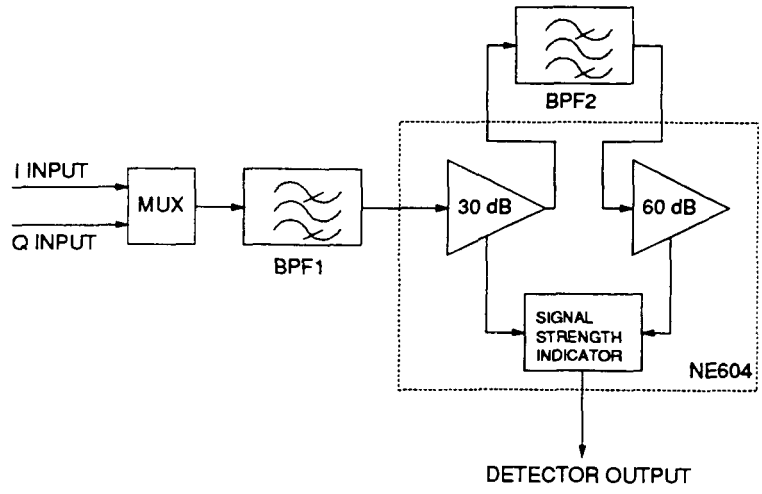

Figure 6.3 Power Detector Block Diagram

The multiplexer reduces the hardware complexity by eliminating the need for two power detectors. Instead, the multiplexer selects one of the I or Q channels to measure. The multiplexer was built from a SGS HC4006 [33] CMOS quad bilateral switch, and used a logic signal from the host PC's parallel port to select between two inputs. Appendix A shows the schematic diagram for the multiplexer.

The bandpass filters are used to select only the part of the 'adjacent channel' part of the spectrum, from 12.5 kHz to 25 kHz with the chosen modulation and data rate. High attenuation is needed to mask out the data signal which can be on the order of 60 dBs higher than the out-of-band power, and thus filters with a fast roll-off, high dynamic range and low noise figure were needed. Passive filters were selected as the most appropriate for the application. Two bandpass filters were used, one a 14^{th} order and the other an 18^{th} order.

The first filter, BPF1, consisted of a 9^{th} order highpass and a 5^{th} order lowpass filter, each designed with 0.1 dB ripple and 50 ohm termination impedances. The simulated fre-

quency response of the BPF1 filter is shown in Figure 6.4 below.

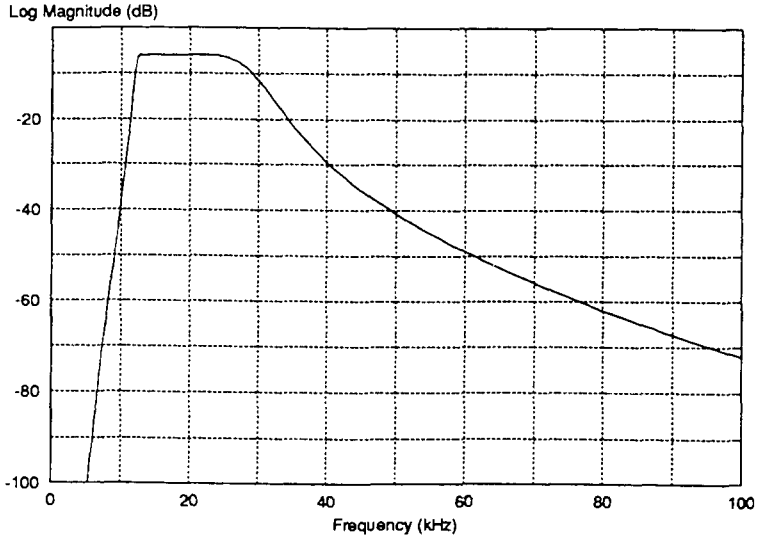

Figure 6.4 BPF1 Frequency Response

The second filter, BPF2, consisted of a 9th order highpass and a 9th order lowpass filter. The highpass was designed for 0.25 dB ripple and 1500 ohm terminations. The lowpass section was designed for 0.05 dB ripple and 1500 ohm terminations. The simulated frequency response of the BPF2 filter is shown in Figure 6.5 below.

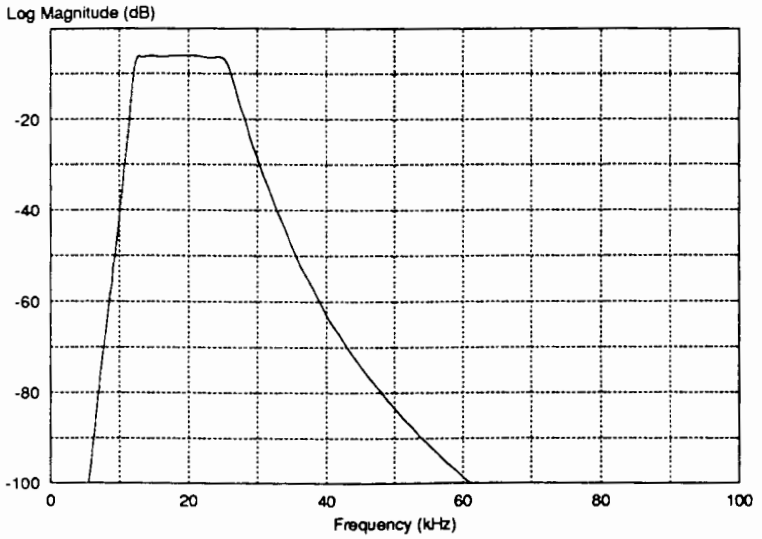

Figure 6.5 BPF2 Frequency Response

The power detector performed well and gave more than 70 dB of dynamic range. However, it was important not to overdrive the first amplifier in the NE604 – harmonics can be generated in the passband of the second filter, BPF2, which will be incorrectly regarded as adjacent channel power.

6.7 Control Circuit

The host AT holding the DSP board acted as the circuit controller. The AT's micro-processor ran a 'C' program which communicated with the DSP board and controlled the power detector multiplexer as depicted below.

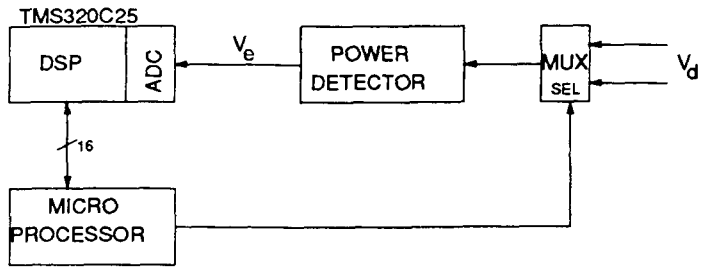

Figure 6.6 Control Circuit Block Diagram

The DSP board read the detector voltage using its ADC and echoed the result to the processor. This echoing was done on a continuous basis, with the micro-processor reading the value only when needed. The micro-processor could also 'write' to the DSP board, controlling both the predistorter and quadrature modulator compensator coefficients.

Section 7 presents the measured results for the system.

7 MEASURED RESULTS

The constructed system was used to test the analytical and simulation results. The results given are (1) surface plots of adjacent channel power versus coefficient mis-adjustment, (2) an example of spectrum improvement achieved with the system, and (3) convergence speed results.

7.1 Adjacent Channel Power Surface Plots

The next two pages show the measured adjacent channel power surface plots. As shown, the quadratic assumption is justified, and well defined minima exist for each of the variables. The figures are in good agreement with the simulation results (Figures 5.4 and 5.5). As in the simulation, mis-adjustment of the fifth order coefficients gives the highest increase in adjacent channel power, followed by the third order coefficients, and then the quadrature modulator DC offset errors, phase error, and finally, the gain imbalance.

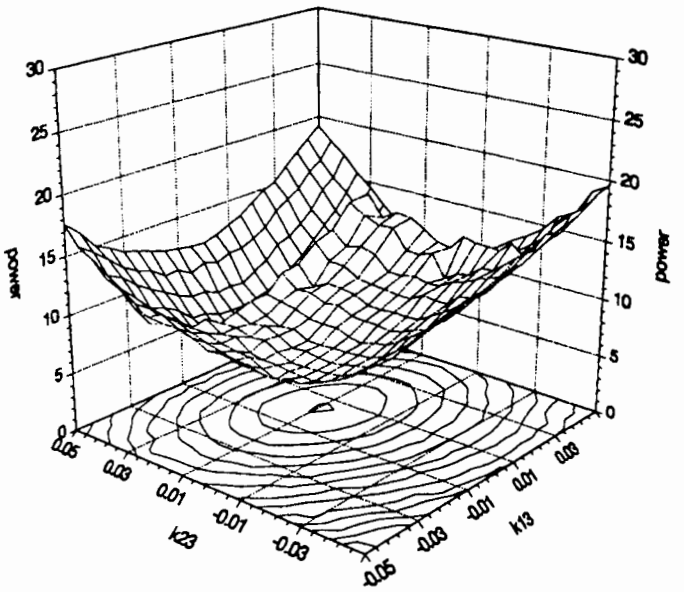

(a) third order coefficients

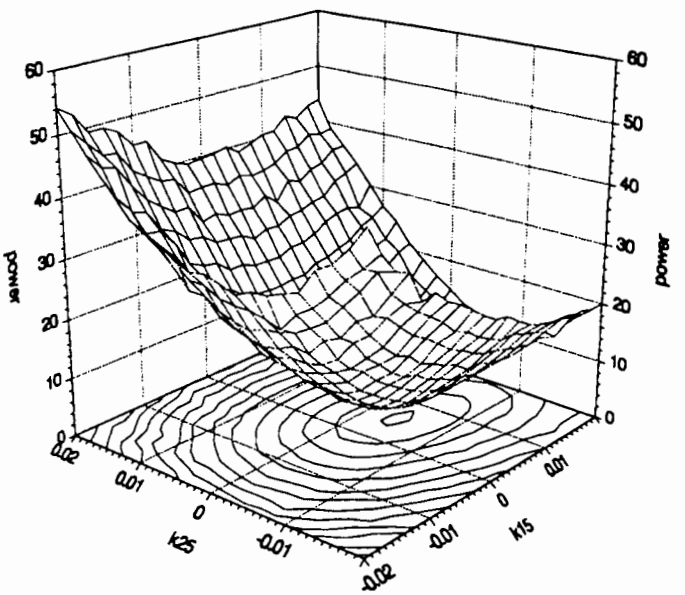

(b) fifth order coefficients

Figure 7.1 Measured Adjacent Channel Power vs Predistorter Coefficients

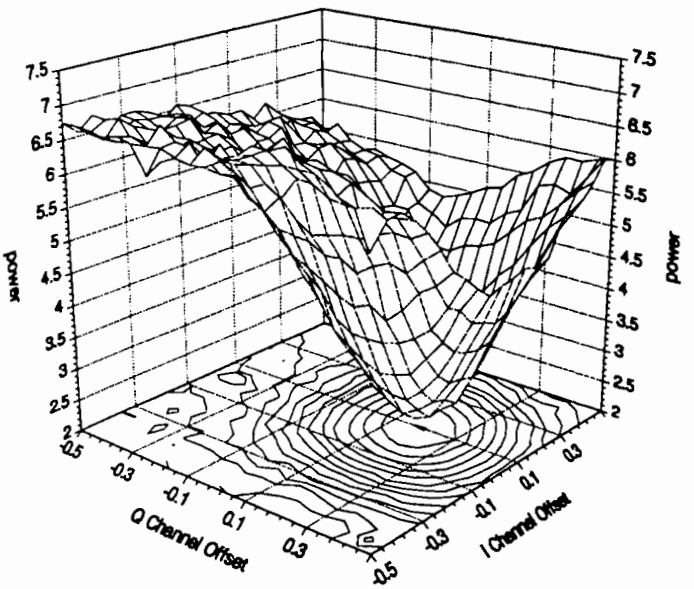

(a) DC voltage offset coefficients

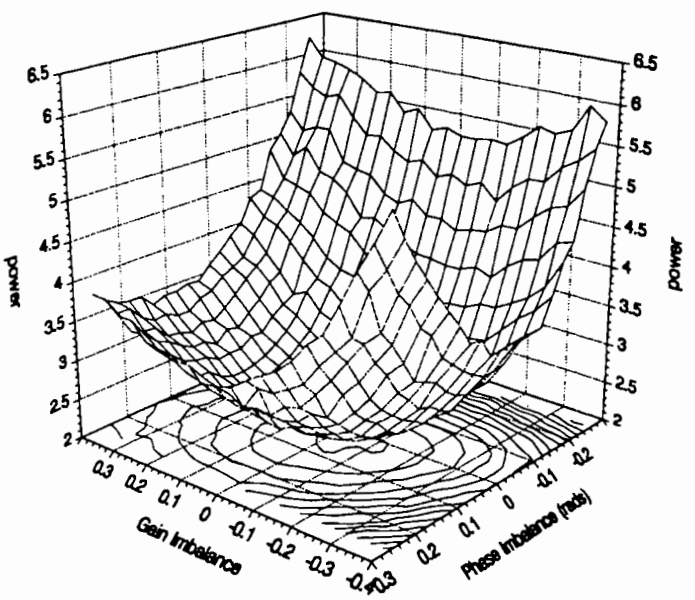

(b) gain and phase coefficients

Figure 7.2 Measured Adjacent Channel Power vs Quadrature Modulator Compensator Coefficients

7.2 Spectrum Improvement

The measured power spectrum is shown in Figure 7.3 below. As shown, the adjacent channel power has been reduced by approximately 20 dB at ±10 kHz offset, the signal edge. As well, the LO leakage at 0 kHz offset is no longer visible. The operating parameters are shown in Table 7.1 on the next page.

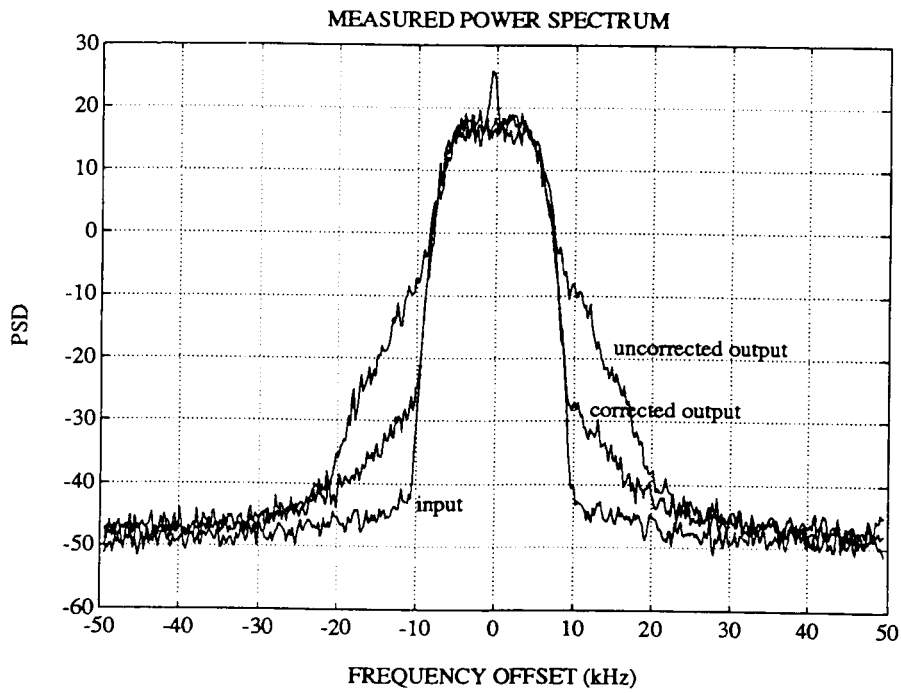

Figure 7.3 Measured Spectrum Improvement

Table 7.1 System Parameters for Measured Results

LO Frequency		850 MHz
Peak Backoff[1]		approximately 1 dB
Power Backoff[2]		approximately 4 dB
Predistorter Coefficients	κ_{11}	0.365
	κ_{21}	0.0
	κ_{13}	-0.006 volt^{-2}
	κ_{23}	0.003 volt^{-2}
	κ_{15}	0.007 volt^{-4}
	κ_{25}	-0.0475 volt^{-4}
gain imbalance,	ε	2 percent
phase error,	φ	0 degrees
DC offsets,	a_1	-0.24 (66% of pulse peak amplitude)
	a_2	0.15 (41% of pulse peak amplitude)

7.3 Convergence Speed

The system converged to the results given in Figure 7.3 (Table 7.1) in about 100 power measurements. Each measurement was made by averaging the detector output over 500 symbols. The convergence time was thus about 3 or 4 seconds as shown in Figure 7.4. Note that with higher symbol rates, the convergence time will decrease proportionally.

---

1 Peak Backoff is defined as (saturation output power / peak output power).

2 Power Backoff is defined as (saturation output power / average output power).

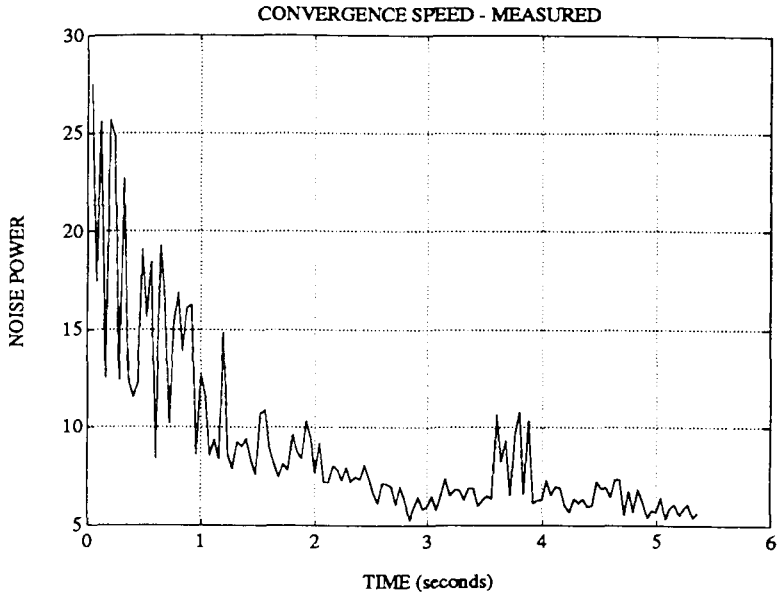

Figure 7.4 Measured Convergence Speed

The time reported in Figure 7.4 does not include the additional time required by the power detector which measured only one channel at a time. Also, a delay was needed in the DSP to set the coefficients in the predistorter and quadrature modulator compensator, and the power detector took several milliseconds to register the correct power reading. The actual convergence time with all these delays was about 15 seconds.

8 CONCLUSIONS

The need for power efficient, spectrum efficient communication systems has driven research towards direct conversion transmitters. The direct conversion architecture provides the potential for smaller, cheaper, more power efficient designs through high frequency quadrature modulators. However, temperature and frequency sensitivities of the quadrature modulators prohibit their use in many situations; the changing gain imbalance, phase error, and DC offsets in the quadrature modulators distort the desired signal.

Linearizers are often used with non-linear amplifiers to get improved power efficiency. But again, temperature, biasing, and frequency dependent characteristics of the amplifier make the system too sensitive to be used.

Several techniques have been used to 'desensitize' linearized power amplifiers and direct conversion architectures. These methods have typically used negative feedback or periodic characterization of the devices to get the desired linearity, but the methods suffer from either instability problems or are inconvenient to use, necessitating periodic interruptions of service.

Stapleton [1], Cavers [2], Kandola [3], and Costescu [4] have demonstrated a power amplifier linearizer using predistortion – a technique in which a nonlinear device with the inverse characteristics of the power amplifier is inserted before the amplifier. Their system is based upon analysis and simulations which show that adjacent channel power is a quadratic function of predistorter mis-adjustment; a measurement of the adjacent channel power is used to control an adaptive predistorter. This type of adaptation does not require fast convergence, since the power amplifier is expected to change slowly with aging and bias changes. The adaptive predistortion system does not have the disadvantages of either instability or the requirement for service interruptions, as do the other methods.

The adaptive transmitter in this thesis is based on the work of Kandola and Cos-

tescu, and includes an adaptive predistorter very similar to Costescu's. However, the new design presented also incorporates an adaptive quadrature modulator compensation circuit to correct for the common problems of direct conversion systems, namely quadrature modulator gain imbalance, phase error, and DC offset errors.

This thesis had three main contributions. First, analysis was presented which showed that the adjacent channel power is a quadratic function of not only predistorter mis-adjustment, but of quadrature modulator errors as well. Second, a new adaptive algorithm which is based on the recursive least-squares algorithm was described. The new algorithm uses the predicted adjacent channel power in a surface-fitting method to get fast convergence. Third, simulation and measured results are presented to confirm the analysis and demonstrate the speed and linearization capabilities of the system. The predistorter and quadrature modulator compensator coefficients converged in roughly three seconds, and an improvement of about 20 dB in adjacent channel power was recorded.

The adaptive system has practical applications in the mobile data communications environment where power efficiency and spectrum efficiency are of prime importance, and also in larger systems where smaller, less expensive power amplifiers can replace larger, less efficient units.

9 REFERENCES

[1] Stapleton, S.P., Cavers, J.K., "A New Technique for Adaptation of Linearizing Predistorters", *Proc. IEEE Vehic. Techn. Conf.*, St. Louis, May 1991.

[2] Cavers, J.K., "Cubic Predistorter: Output Spectrum and Error Surface", private correpondence, May 1990.

[3] Kandola, G., *Analysis and Simulation of an Adaptive Predistorter*, M.A.Sc. Thesis, School of Engineering Science, SFU, 1991.

[4] Costescu, F., *Amplifier Linearization Using Adaptive Analog Predistortion*, M.A.Sc. Thesis, School of Engineering Science, SFU, 1991.

[5] Shanmugan, K.S. And Breipohl, A.M., *Random Processes: Detection, Estimation and Data Analysis*, John Wiley & Sons, New York, 1988.

[6] Hewlett-Packard Company, 8600 Soper Hill Road, Everett, WA 98205-1298 U.S.A.

[7] Rambaran, S., Hilborn, D., *I/Q Modulators*, Communications Science Laboratory, Simon Fraser University, 1992.

[8] Faulkner, M., Mattsson, T., Yates, W., "Automatic Adjustment of Quadrature Modulators", *Electronics Letters*, Vol.27, No.3, pp. 214-216, 31 January 1991.

[9] Telliez, I. et al, "A Compact, Monolithic Microwave Demodulator-Modulator for 64 QAM Digital Radio Links", *IEEE Transactions on Microwave theory and Techniques*, Vol.39, No.12, pp. 1947-1953, December 1991.

[10] Bateman, A., Haines, D., Wilkinson, R., "Direct Conversion Linear Transceiver Design", *IEE Fifth International Conference on Mobile Radio and Personal Communications*, pp. 53-56, 1989.

[11] Green, D.R.Jr., "Characterization and compensation of Nonlinearities in Microwave Transmitters", *IEEE Trans.*, pp. 213-217, 1982.

[12] Casadevall, F.J., "The LINC Transmitter", *RF Design*, pp.41-48, February 1990.

[13] Nagata, Y., "Linear Amplification Technique for Digital Mobile Communications", *Proc. IEEE Vehic. Tech. Conf.*, pp. 159-164, San Fransisco, 1989.

[14] Cavers, J.K., "A Linearizing Predistorter with Fast Adaptation", *40th Vehic. Tech. Conf.*, IEEE Cat. 90CH2864-4, pp. 41-47.

[15] Jacoby, S.L.S., Kowalik, J.S., and Pizzo, J.T., *Iterative Methods for Nonlinear Optimization Problems*, New Jersey, Prentice-Hall, 1972.

[16] Peressini, A.L., Sullivan, F.E., and Uhl, J.J. Jr., *The Mathematics of Nonlinear Programming*, New York: Springer-Verlag, 1988.

[17] Lathi, B.P., *Modern Digital and Analog Communication Systems, 2nd Ed.*, Holt, Rinehart and Winston, Philadelpia, 1989.

[18] Proakis, J., *Digital Communications*, McGraw-Hill Book Company, pp. 110-112, 1983.

[19] Wozencraft and Jacobs, *Principles of Communication Engineering*, McGraw-Hill Book Company, pp.205-206, 1966.

[20] Private correspondence with J.K. Cavers, "Predistorter Coefficient Optimization by Surface Fit", February 12, 1992.

[21] Proakis, J.G., Manolakis, D.G., *Introduction to Digital Signal Processing*, Macmillan Publishing, New York, pp. 888-897, 1988.

[22] Haykin, S.S., *Adaptive Filter Theory*, Prentice-Hall, New Jersey, pp. 385-387, 1986.

[23] Oppenheim, A.V., Schafer, R.W., *Discrete-Time Signal Processing*, Prentice-Hall, New Jersey, pp. 450-453, 1988.

[24] 3dbm Inc., Westlake Village, CA.

[25] Atlanta Signal Processors Inc., 770 Spring Street, Suite 208, Atlanta, Georgia 30308.

[26] Texas Instruments, 9100 Southwest Frwy., Suite 237, Houston, TX 77036.

[27] SPECTRUM Signal Processing Inc., #301-3700 Gilmore Way, Burnaby, B.C., V5G 4M1.

[28] Mini-Circuits, Brooklyn, New York.

[29] Burr-Brown Corporation, 6730 S. Tucson Blvd., Tucson, AZ 85706.

[30] Niewiadomski, S., *Filter Handbook*, Heinemann Professional Publishing, Oxford, 1989, pp. 78.

[31] Signetics, 811 East Arques Ave., P.O. Box 3409, Sunnyvale, CA 94088-3409.

[32] Signetics, *Linear Data Manual, Volume 1: Communications*, 1987, pp. 4-140 to 4-142.

[33] SGS-Semiconductors Corporation, 1000 East Bell Road, Pheonix, AZ 85022.

APPENDIX A: HARDWARE SCHEMATICS

This appendix is used to show the different circuits used in the implemented system. In total, six schematics are shown, including the reconstruction lowpass filter, the quadrature modulator, and the detector circuit including the multiplexer and bandpass filters.

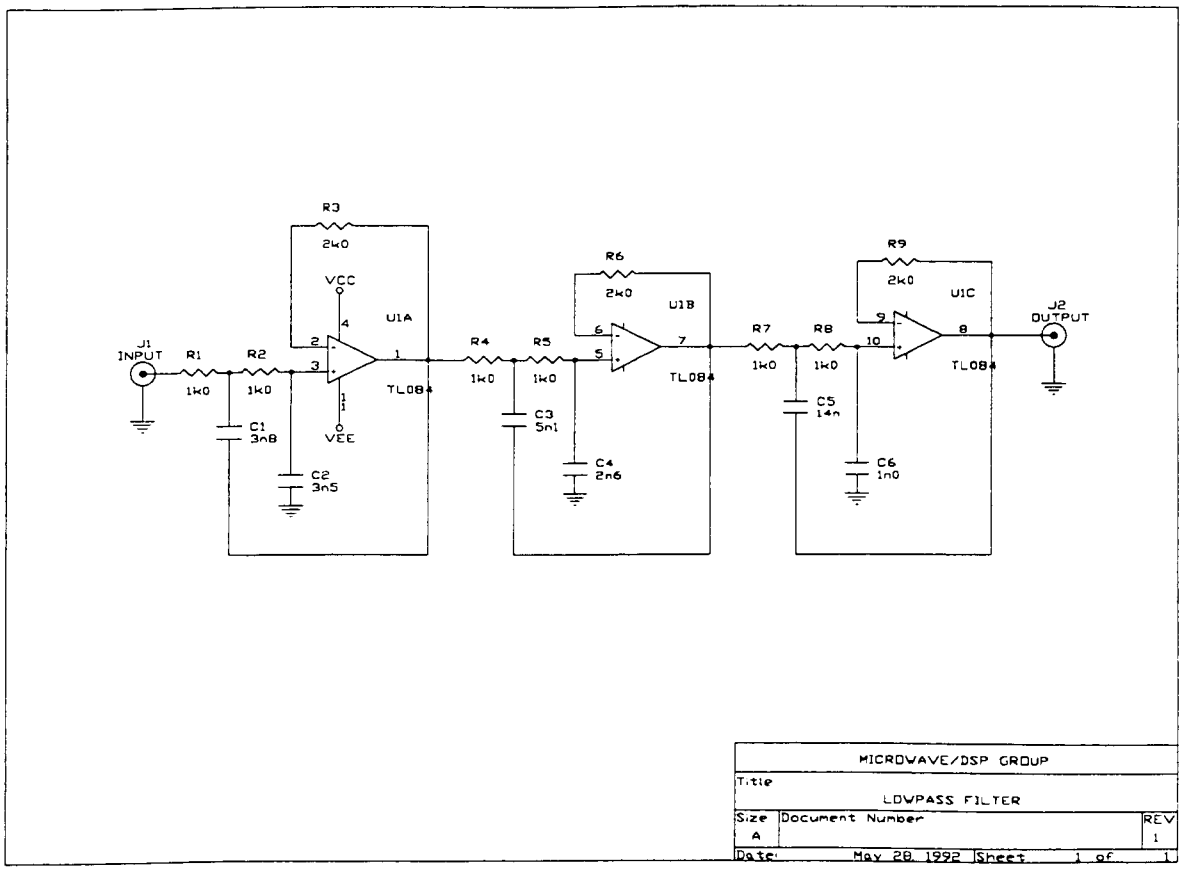

Figure A1 Lowpass Filter for Digital-to-Analog Conversion

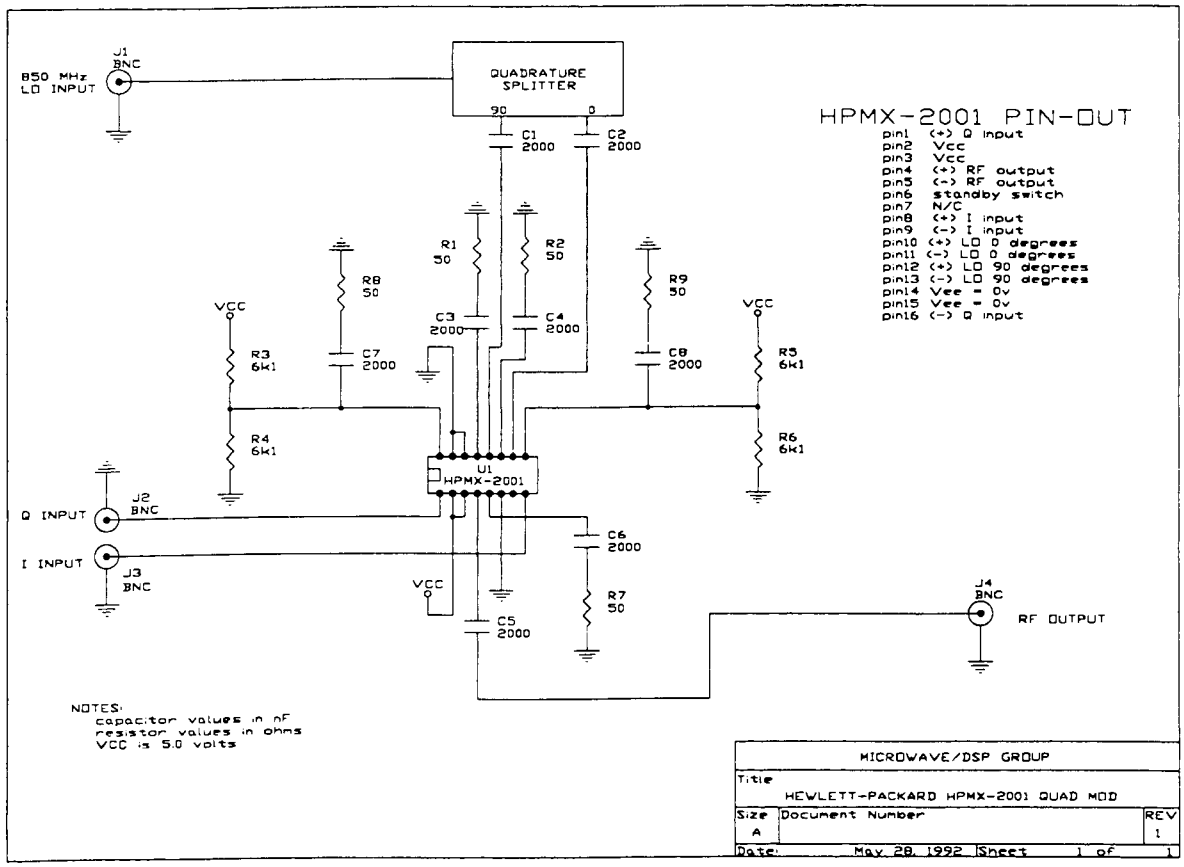

Figure A2 Hewlett-Packard Quadrature Modulator

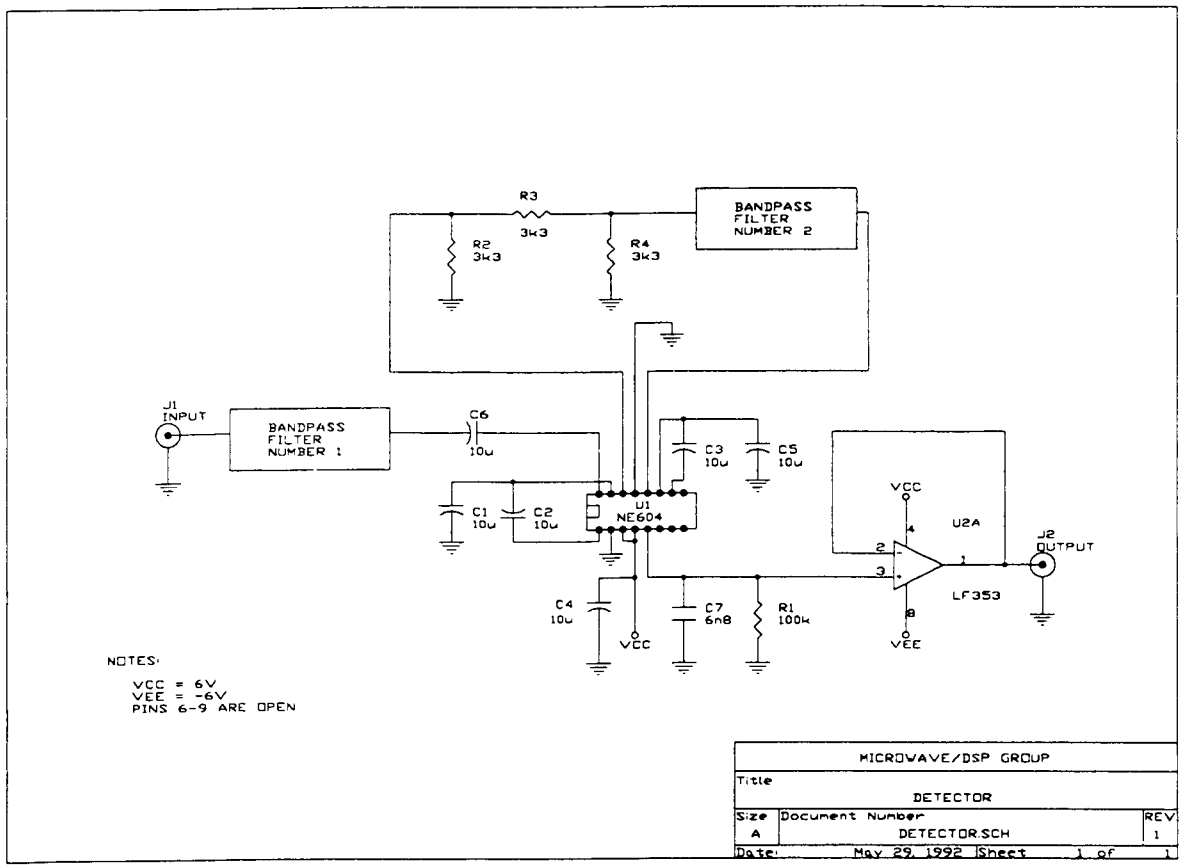

Figure A3 Detector Circuit

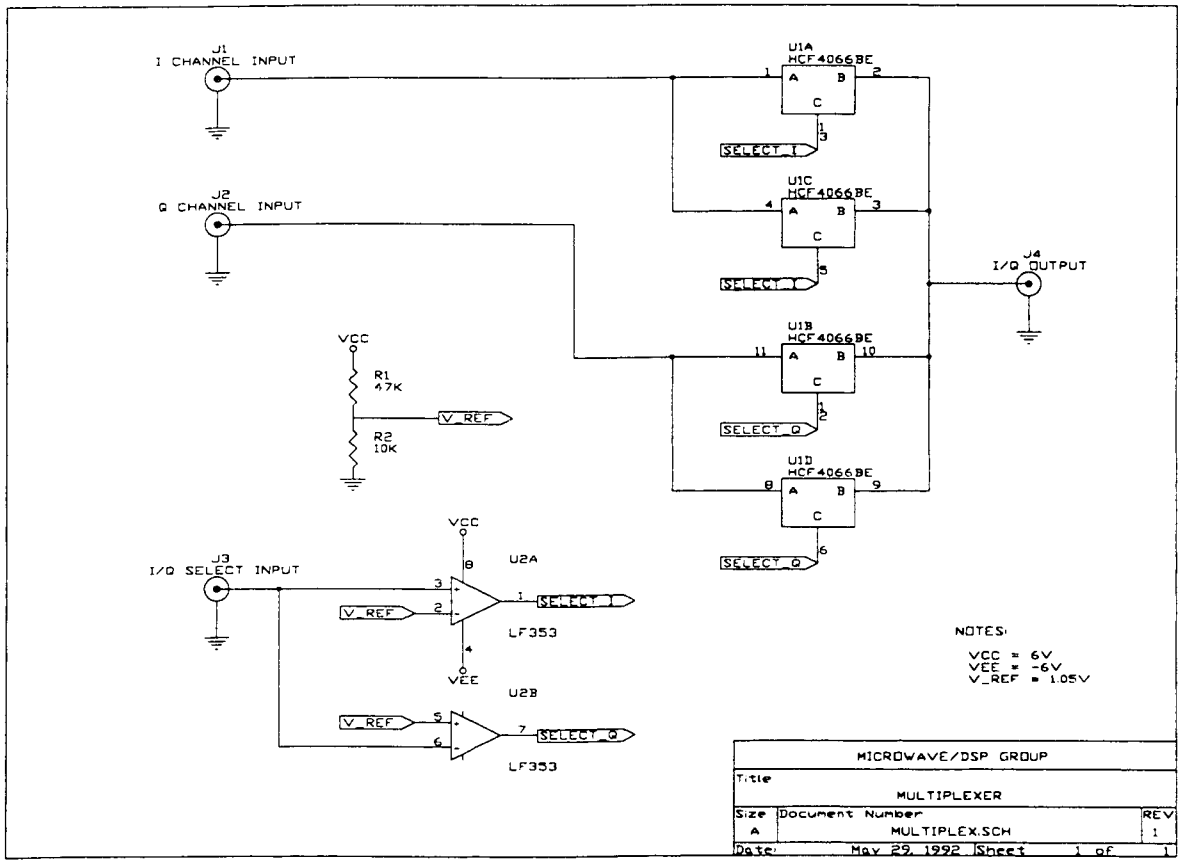

Figure A4 Multiplexer Circuit

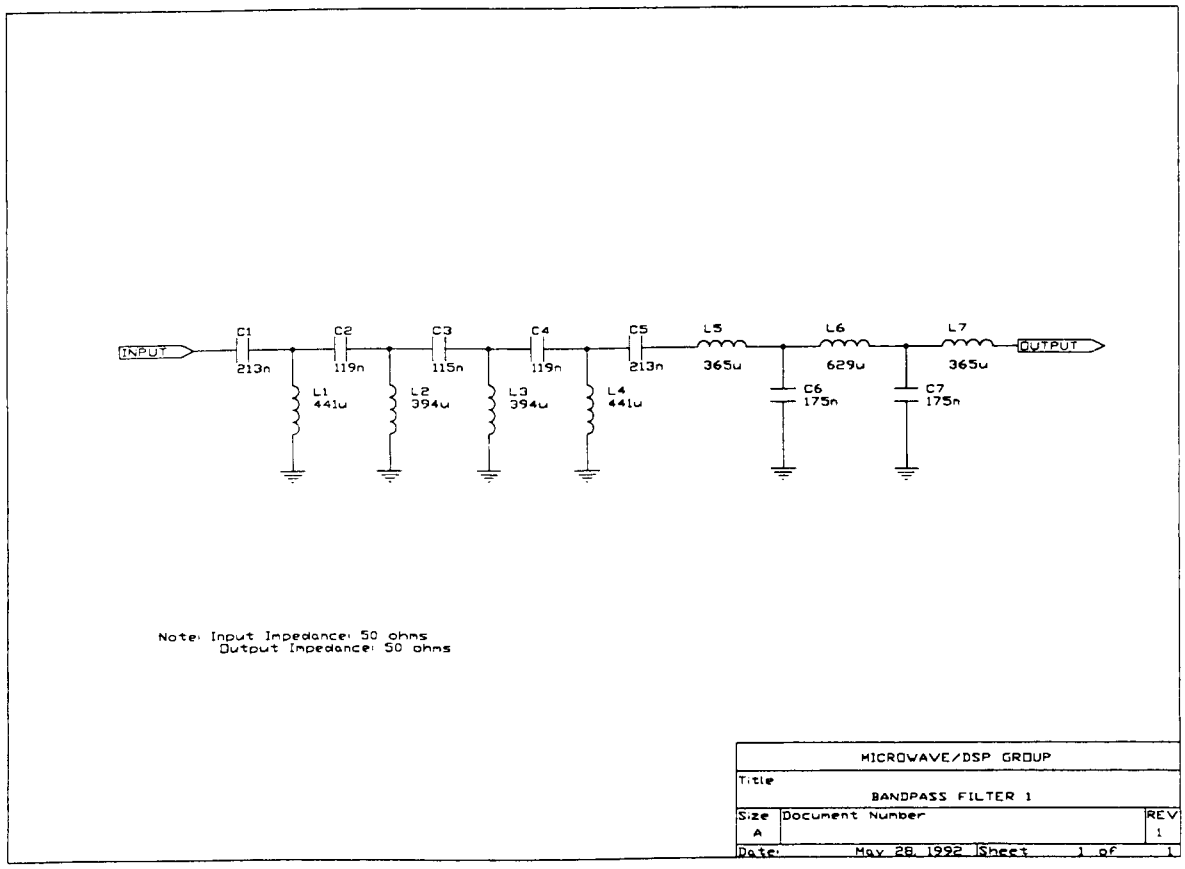

Figure A5 Bandpass Filter 1 (BPF1)

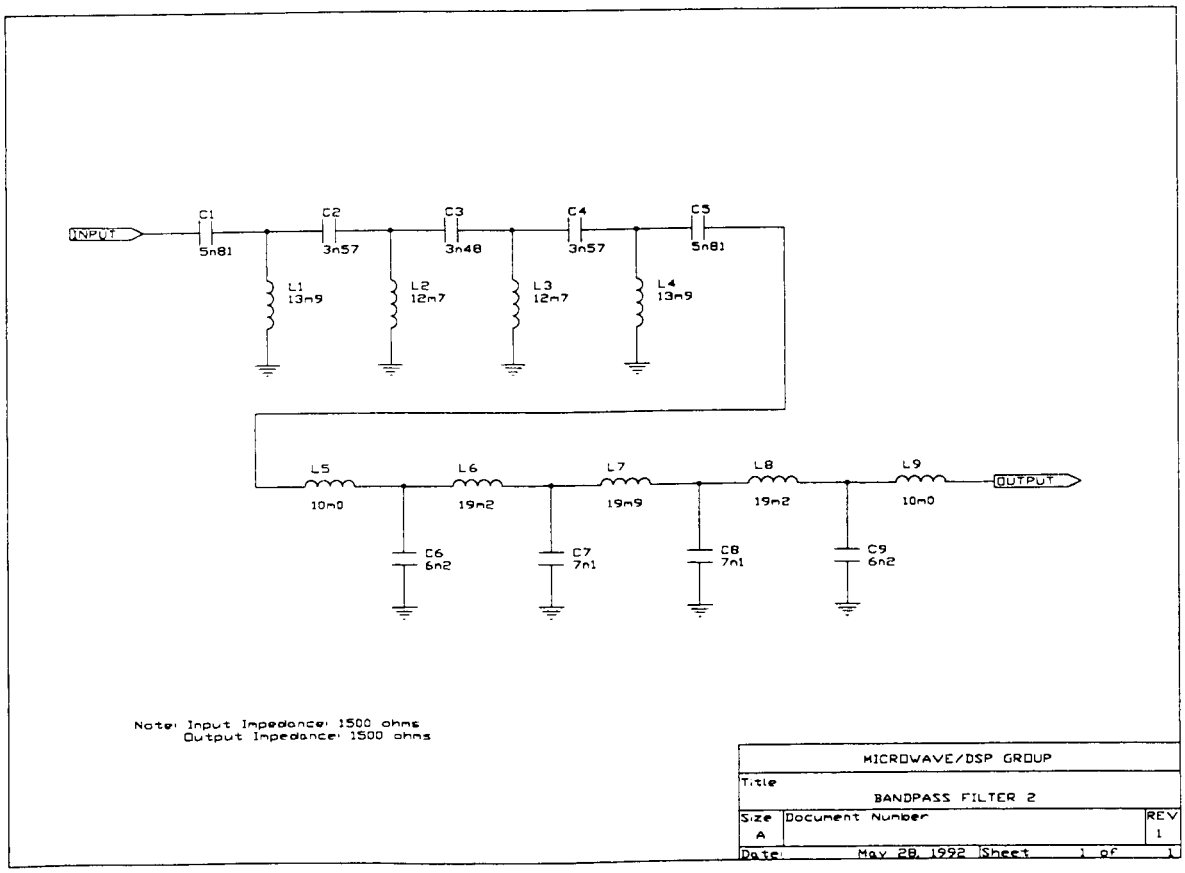

Figure A6 Bandpass Filter 2 (BPF2)

APPENDIX B: GAUSSIAN EXPANSION RESULTS

This section gives the power amplifier autocorrelation function for a Gaussian, zero-mean, stationary input signal, $R_m(\tau)$. As discussed in Section 3.3, the desired correlation function is the sum of several expectations:

$$\begin{aligned} 2R_a(\tau) = & \zeta_1\zeta_1^* E\{V_1 V_2^*\} \\ & + \zeta_1\zeta_3^* E\left\{V_1 V_2 V_2^{*2}\right\} \\ & + \zeta_1^*\zeta_3 E\{V_1^2 V_1^* V_2^*\} \\ & + \zeta_3\zeta_3^* E\left\{V_1^2 V_1^* V_2 V_2^{*2}\right\}. \end{aligned}$$

where $V_a(t) = V_q(t)\left[\zeta_1 + \zeta_3 |V_q(t)|^2\right]$,

$V_a^*(t+\tau) = V_q^*(t+\tau)\left[\zeta_1^* + \zeta_3^* |V_q(t+\tau)|^2\right]$.

The four expectations are given below, followed by their (suitably scaled) sum. The scalars A, B, C, D, μ_1, and μ_2 are

$$A = \alpha^2 \cos^2\left(\frac{\phi}{2}\right) + \beta^2 \sin^2\left(\frac{\phi}{2}\right) \approx 1 + \varepsilon$$

$$B = \alpha^2 \sin^2\left(\frac{\phi}{2}\right) + \beta^2 \cos^2\left(\frac{\phi}{2}\right) \approx 1 - \varepsilon$$

$$C = \sin(\phi) \approx \phi$$

$$D = \alpha\beta\cos(\phi) \approx 1 - \frac{\varepsilon^2 + \phi^2}{2}$$

$$\mu_1 = a_1\alpha\cos\left(\frac{\phi}{2}\right) + a_2\beta\sin\left(\frac{\phi}{2}\right) \approx a_1$$

$$\mu_2 = a_1\alpha\sin\left(\frac{\phi}{2}\right) + a_2\beta\cos\left(\frac{\phi}{2}\right) \approx a_2$$

FIRST EXPECTATION

$$E\{V_1 V_2^*\} = 2R_{ii}(\tau) - j2DR_{iq}(\tau) + \mu_1^2 + \mu_2^2$$

SECOND EXPECTATION

$$E\{V_1V_2V_2^{*2}\} = R_m(0)R_{ii}(\tau)[12 - 4AB + 4C^2]$$
$$+[R_{ii}(\tau) + R_m(0)][2\mu_1^2(1+A) + 2\mu_2^2(1+B) + 4\mu_1\mu_2C]$$
$$+(\mu_1^2 + \mu_2^2)^2$$
$$+j\{R_m(0)R_{iq}(\tau)[-8D]$$
$$+[R_{ii}(\tau) - R_m(0)][2C(\mu_1^2 - \mu_2^2) - 2\mu_1\mu_2(A-B)]$$
$$+R_{iq}(\tau)[-4D(\mu_1^2 + \mu_2^2)]\}$$

THIRD EXPECTATION

$$E\{V_1^2V_1^*V_2^*\} = R_m(0)R_{ii}(\tau)[12 - 4AB + 4C^2]$$
$$+[R_{ii}(\tau) + R_m(0)][2\mu_1^2(1+A) + 2\mu_2^2(1+B) + 4\mu_1\mu_2C]$$
$$+(\mu_1^2 + \mu_2^2)^2$$
$$+j\{R_m(0)R_{iq}(\tau)[-8D]$$
$$+[R_{ii}(\tau) - R_m(0)][-2C(\mu_1^2 - \mu_2^2) + 2\mu_1\mu_2(A-B)]$$
$$+R_{iq}(\tau)[-4D(\mu_1^2 + \mu_2^2)]\}$$

FOURTH EXPECTATION

$$E\{V_1^2 V_1^* V_2 V_2^{*2}\} =$$

$$R_m(0)^2 R_{ii}(\tau)\,[9(A^3+B^3)+14AB+40C^2]$$

$$+R_{ii}(\tau)^3\,[6(A^3+B^3)+4AB+32C^2]$$

$$+R_{ii}(\tau)R_{iq}(\tau)^2\,[16D^2]$$

$$+R_m(0)R_{ii}(\tau)\,[(\mu_1^2+\mu_2^2)(16C^2+8AB+6(A^2+B^2))+12(\mu_1^2A^2+\mu_2^2B^2)]$$

$$+R_m(0)^2\,[4(A+1)^2\mu_1^2+4(B+1)^2\mu_2^2+32\mu_1\mu_2C]$$

$$+R_{ii}(\tau)^2\,[8(1+4C^2)(\mu_1^2+\mu_2^2)+16A^2\mu_1^2+16B^2\mu_2^2+64\mu_1\mu_2C]$$

$$+R_{iq}(\tau)^2\,[8(\mu_1^2+\mu_2^2)D^2]$$

$$+R_m(0)\,[4(\mu_1^4+\mu_2^4)+16\mu_1^2\mu_2^2+4\mu_1^4A+4\mu_2^4B+8\mu_1\mu_2(\mu_1^2+\mu_2^2)C]$$

$$+R_{ii}(\tau)\,[2(\mu_1^4+\mu_2^4)+8(\mu_1^4A+\mu_2^4B)+20\mu_1^2\mu_2^2+16\mu_1\mu_2(\mu_1^2+\mu_2^2)C]$$

$$+\left[(\mu_1^2+\mu_2^2)^3\right]$$

$$+j[R_m(0)^2R_{iq}(\tau)\,[-D(24+8AB-8C^2)]$$

$$+R_{ii}(\tau)^2R_{iq}(\tau)\,[-12D(A^2+B^2)-32C^2D+8ABD]$$

$$+R_{iq}(\tau)^3\,[-16D^3]$$

$$+R_{iq}(\tau)R_m(0)\,[-40D(\mu_1^2+\mu_2^2)+8D(A\mu_1^2+B\mu_2^2)+16\mu_1\mu_2CD]$$

$$+R_{ii}(\tau)R_{iq}(\tau)\,[16(\mu_1^2+\mu_2^2)D-32(\mu_1^2A^2+\mu_2^2B^2)D-64\mu_1\mu_2CD]$$

$$+R_{iq}(\tau)\left[-6(\mu_1^2+\mu_2^2)^2D\right]]$$

The previous four results are combined to give $R_a(\tau)$ as the amplifier output autocorrelation function:

$$R_a(\tau) = |\zeta_1|^2 \left\{ R_{ii}(\tau) + \frac{\mu_1^2 + \mu_2^2}{2} - jDR_{iq}(\tau) \right\}$$

$$+2Re(\zeta_1 \zeta_3^*) \{ R_m(0) R_{ii}(\tau) [6 - 2AB + 2C^2] + R_{ii}(\tau) [\mu_1^2(1+A) + \mu_2^2(1+B) + 2\mu_1\mu_2 C]$$

$$+R_m(0) [\mu_1^2(1+A) + \mu_2^2(1+B) + 2\mu_1\mu_2 C] + \frac{1}{2}(\mu_1^2 + \mu_2^2)^2 \}$$

$$+j2Re(\zeta_1 \zeta_3^*) \{ R_m(0) R_{iq}(\tau) [-4D] + R_{iq}(\tau) - 2D(\mu_1^2 + \mu_2^2)] \}$$

$$+j2Im(\zeta_1 \zeta_3^*) \{ R_{ii}(\tau) [C(\mu_1^2 - \mu_2^2) - \mu_1\mu_2(A - B)] + R_m(0) [-C(\mu_1^2 - \mu_2^2) + \mu_1\mu_2(A - B)] \}$$

$$+|\zeta_3|^3 \{ R_m(0)^2 R_{ii}(\tau) \left[\frac{9}{2}(A^3 + B^3) + 7AB + 4DC^2 \right]$$

$$+R_{ii}(\tau)^3 [3(A^3 + B^3) + 2AB + 16C^2] + R_{ii}(\tau) R_{iq}(\tau)^2 [8D^2]$$

$$+R_m(0) R_{ii}(\tau) [(\mu_1^2 + \mu_2^2)(8C^2 + 4AB + 3A^2 + 3B^2) + 6(\mu_1^2 A^2 + \mu_2^2 B^2)]$$

$$+R_m(0)^2 [2(A+1)^2 \mu_1^2 + 2(B+1)^2 \mu_2^2 + 16\mu_1\mu_2 C]$$

$$+R_{ii}(\tau)^2 [4(1 + 4C^2)(\mu_1^2 + \mu_2^2) + 8A^2\mu_1^2 + 8B^2\mu_2^2 + 32\mu_1\mu_2 C]$$

$$+R_{iq}(\tau)^2 [4(\mu_1^2 + \mu_2^2) D]$$

$$+R_m(0) 2(\mu_1^4 + \mu_2^4) + 8\mu_1^2\mu_2^2 + 2\mu_1^4 A + 2\mu_2^4 B + 4\mu_1\mu_2(\mu_1^2 + \mu_2^2) C]$$

$$+R_{ii}(\tau) [(\mu_1^4 + \mu_2^2) + 4(\mu_1^4 A + \mu_2^4 B) + 10\mu_1^2\mu_2^2 + 8\mu_1\mu_2(\mu_1^2 + \mu_2^2) C]$$

$$+(1/2)(\mu_1^2 + \mu_2^2)^3 \}$$

$$+j|\zeta_3|^2 \{ R_m(0)^2 R_{iq}(\tau) [-D(12 + 4AB - 4C^2)]$$

$$+R_{ii}(\tau) R_{iq}(\tau) [-6D(A^2 + B^2) - 16C^2 D + 4ABD] + R_{iq}(\tau)^3 [-8D^3]$$

$$+R_{iq}(\tau) R_m(0) [-20D(\mu_1^2 + \mu_2^2) + 4D(A\mu_1^2 + B\mu_2^2) + 8\mu_1\mu_2 CD]$$

$$R_{ii}(\tau) R_{iq}(\tau) [8(\mu_1^2 + \mu_2^2) D - 16(\mu_1^2 A + \mu_2^2 B) D - 32\mu_1\mu_2 CD]$$

$$R_{iq}(\tau) \left[-3(\mu_1^2 + \mu_2^2)^2 D \right] \}$$